

2008

Characterization of ferroelectric material for advanced RF circuit design

Jiadong Wang
University of Dayton

Follow this and additional works at: https://ecommons.udayton.edu/graduate_theses

Recommended Citation

Wang, Jiadong, "Characterization of ferroelectric material for advanced RF circuit design" (2008).
Graduate Theses and Dissertations. 6226.
https://ecommons.udayton.edu/graduate_theses/6226

This Thesis is brought to you for free and open access by the Theses and Dissertations at eCommons. It has been accepted for inclusion in Graduate Theses and Dissertations by an authorized administrator of eCommons. For more information, please contact mschlangen1@udayton.edu, ecommons@udayton.edu.

Characterization of Ferroelectric Material for Advanced RF Circuit Design

Thesis

Submitted to

The School of Engineering of the
UNIVERSITY OF DAYTON

In Partial Fulfillment of the Requirements for

The Degree

Master of Science in Electrical Engineering

By

Jiadong Wang

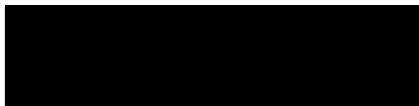
UNIVERSITY OF DAYTON

Dayton, Ohio

May, 2008

CHARACTERIZATION OF FERROELECTRIC MATERIAL FOR ADVANCED RF
CIRCUIT DESIGN

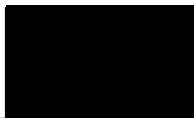
APPROVED BY



Guru Subramanyam
Advisory Committee Chairman
Associate Professor, Department of
Electrical and Computer Engineering



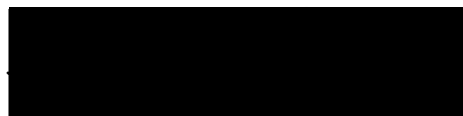
Robert Penno
Committee Member
Associate Professor, Department of
Electrical and Computer Engineering



Partha Banerjee
Committee Member
Professor, Department of Electrical
and Computer Engineering, and
Electro-Optics Program



Malcolm W. Daniels, PhD.
Associate Dean
School of Engineering



Joseph E. Saliba, PhD., P.E.
Dean
School of Engineering

©Copyright by

Jiadong Wang

All rights reserved

2008

ABSTRACT

CHARACTERIZATION OF FERROELECTRIC MATERIALS FOR ADVANCED RF CIRCUIT DESIGN

Name: Wang, Jiadong

University of DAYTON

Advisor: Dr. Guru Subramanyam

This research is focused on investigating electrical properties of novel electronic materials such as ferroelectric thin films for RF and microwave circuit design. The ferroelectric materials are used as nonlinear voltage tunable dielectrics for variable capacitors (varactors). Capacitors made using the ferroelectric thin films are tested using a Radiant tester with Vision Software at low frequencies (<1 MHz) and a vector network analyzer with Microwave Office Simulation Package at GHz frequencies. Polarization versus electric field (P-E, Hysteresis loop), leakage current versus applied voltage (I-V) and capacitance versus applied voltage (C-V) are the three main characteristics for the ferroelectric thin films which have been measured on different materials. By using different drive profile as the input signal, we found the differences between AC & DC resistance of Lead Zirconium Titanate (PZT) ferroelectric capacitors. Microwave characterization of the ferroelectric capacitors was done using the varactor shunt switch structure, and measuring the scattering parameters. The feasibility of a rapid bio-enabled approach to form ferroelectric Barium Titanate (BaTiO_3) at room temperature from an aqueous salt solution at near neutral pH was demonstrated by collaborating with Georgia Tech. Also research on the frequency tunable antenna integrated with shunt switch ferroelectric varactor has been initiated and simulation results are presented.

ACKNOWLEDGEMENT

I enjoyed my study and research very much since I joined the research group led by Prof. Guru Subramanyam. So my greatest gratitude would be extended to my advisor, Prof. Guru Subramanyam, for his constant support and valuable instruction. Without his direct guidance, I cannot complete my graduate study in UD so well. Besides his expertise in the relevant area, his dedication to electrical engineering contributes to my life long development, which is far beyond a master's thesis. I will always appreciate it.

I would like to express my gratitude to other committee members, Prof. Robert Penno and Prof. Partha Banerjee for helpful discussions and kind motivations. I would like to extend my thanks to current and former PhD students in our group Mark Patterson, Huadong, Li, Carrie M. Bartsch, and Faruque Ahamed since they helped me during the research. Additionally, I must give thanks to Hai Jiang from Dr. Pasala's group, Yaodong Yang from Dr. Liming Dai's group, who have given me help both through daily life and academic discussions.

And last, but not least, I am grateful for the support of my girlfriend, Fang Ma who is currently in National University of Singapore and my family in Xi'an, thousands of miles away from Dayton. They always give me spiritual support and encouragement to accomplish the task.

TABLE OF CONTENTS

ACKNOWLEDGEMENT.....	v
TABLE OF CONTENTS.....	vi
LIST OF FIGURES.....	ix
CHAPTER	
1. INTRODUCTION.....	1
1.1 Ferroelectric materials.....	1
1.1.1 Overview of ferroelectrics.....	1
1.1.2 Origin of ferroelectrics.....	2
1.1.3 Applications of ferroelectrics.....	2
1.1.4 Barium Strontium Titanate.....	3
1.2 Electrical properties of ferroelectric material.....	4
1.2.1 Hysteresis loop.....	4
1.2.2 Permittivity – electric field ($\epsilon - V$ or $C - V$) relationship.....	5
1.2.3 Current vs voltage (I-V).....	5
1.3 Microwave applications of ferroelectric materials.....	6
1.3.1 Review of ferroelectric microwave applications.....	6
1.3.2 Frequency tunable antenna.....	9
1.4 Objective of the study.....	10
1.5 Significance of the study.....	11
1.6 Organization of the thesis.....	11

2. ELECTRICAL CHACRACTERIZATION TECHNIQUES AND EXPERIMENTAL SETUP	13
2.1 Introduction to electrical characterization techniques.....	13
2.2 Electrical properties characterization system.....	14
2.3 Samples.....	16
2.3.1 Standard capacitors.....	16
2.3.2 Wafer based samples.....	17
2.3.3 Bulk materials.....	17
2.4 Low frequency measurement (< 1MHz).....	17
2.4.1 Hysteresis loop.....	18
2.4.2 C-V measurement.....	20
2.4.3 I-V measurement.....	23
2.5 Microwave frequency measurement (> 1 GHz).....	26
2.5.1 Capacitive test structure to characterize electronic thin films.....	27
3. RF POWER CONVERTER CIRCUIT DESIGN.....	30
3.1 Overview of wireless microwave power transmission technology.....	30
3.2 Patch antenna design.....	32
3.2.1 Basic patch antenna design.....	32
3.2.2 Patch antenna impedance match to a 50 Ω feed line.....	34
3.3 Schematic power converter circuit design.....	37
3.4 Impedance matching circuit design.....	38
3.5 Results and measurements.....	41
3.5.1 Design of the microstrip patch antenna with matching impedance.....	41

3.5.2 Diode impedance characterization.....	44
3.5.3 Impedance matching microstrip.....	46
3.5.4 Circuit performance as a rectifier.....	47
4. FREQUENCY TUNABLE ANTENNA DESIGN USING VARACTOR TECHNOLOGY.....	51
4.1 Motivation	51
4.2 Electrical equivalent model.....	53
4.3 Electromagnetic layout.....	55
4.4 Simulation results of electrical equivalent model.....	56
5. EXPERIMENTAL RESULTS ON FERROELECTRIC THIN FILMS AND DEVICES.....	58
5.1 Electrical characterization for advanced electronic materials.....	58
5.1.1 Comparison of AC & DC resistance for PZT thin film capacitor.....	58
5.1.2 Hysteresis loop of the BT ₂ peptide-induced BaTiO ₃	65
5.1.3 Leakage current measurement for fiber nanotube junction.....	67
5.2 RF performance of varactor shunt	68
5.2.1 Frequency dependent impedance relationship of varactor shunt switch..	68
5.2.2 Temperature dependent performance of varactor shunt switch	71
5.2.3 Dielectric property of BST thin film based on varactor shunt switch	74
VI. SUMMARY AND FUTURE WORK.....	77
6.1 Summary.....	77
6.2 Future work	78

LIST OF FIGURES

<u>Figure</u>	<u>Page</u>
2.1 Low frequency characterization system setup	15
2.2 Microwave frequency characterization system setup	15
2.3 Radiant socket board	16
2.4 Sawyer tower circuit	18
2.5 A simple experimental setup for hysteresis loop measurement	19
2.6 Demonstration of hysteresis loop setup	20
2.7 Demonstration of C-V measurement sample setup.....	21
2.8 Demonstration of C-V measurement drive profile setup.....	22
2.9 Demonstration of I-V measurement setup	25
2.10 Demonstration of I-V measurement drive profile setup	25
2.11 Three dimensional view of capacitive test structure	28
2.12 The electrical model for the capacitive test structure	29
3.1 Schematic antenna rectifying system.....	31
3.2 Physical and effective lengths of rectangular microstrip patch.....	33
3.3 Equivalent circuit transmission-line model.....	34
3.4 Recessed microstrip-line patch antenna.....	36
3.5 Simple antenna rectifying circuit	38
3.6 Schematic view of microstrip waveguide for rectifying circuit.....	38
3.7 Simple-stub matching circuit.....	39

3.8 Frequency response of return loss S11 for patch antenna.....	42
3.9 Dimensions of designed 2.45 GHz antenna.....	43
3.10 Frequency response of impedance amplitude for patch antenna.....	43
3.11 Frequency response of impedance phase angle for patch antenna.....	44
3.12 Linear model for a diode chip.....	45
3.13 Model of the SOT-23 package.....	45
3.14 Three dimensional view of microstrip waveguide.....	46
3.15 Physical characteristics of microstrip waveguide.....	47
3.16 Schematic circuit of rectifier antenna.....	48
3.17 Simulation results for schematic equivalent circuits.....	49
3.18 Top view of the rectifier antenna layout.....	49
3.19 Measurement results at low frequency 15 MHz.....	50
4.1 Schematic view of the frequency tunable microstrip patch antenna.....	52
4.2 Top view of ferroelectric shunt switch based on varactor technology.....	53
4.3 Equivalent electrical model for antenna.....	54
4.4 Equivalent electrical model for ferroelectric varactor.....	54
4.5 A sketch of tunable antenna integrated with ferroelectric varactor.....	55
4.6 Equivalent electrical circuit of the tunable frequency antenna.....	56
4.7 Simulation results of S11 for the electrical equivalent circuit of tunable frequency antenna.....	57
5.1 Drive profile of AC small signal measurement.....	59
5.2 Drive profile of DC small signal measurement.....	59
5.3 Cross section of a ferroelectric capacitor on a silicon wafer.....	60

5.4 Drive profile for resistance measurement by radiant tester.....	61
5.5 C-V curve of the PZT thin film capacitor.....	62
5.6 DC resistance of the PZT thin film capacitor.....	63
5.7 An equivalent circuit for ferroelectric thin film capacitor.....	64
5.8 AC resistance of the PZT thin film capacitor.....	64
5.9 Polarization versus applied electric field at 1kHz for the peptide-induced BaTiO ₃ ...	67
5.10 I-V curve of fiber nanotube junction.....	68
5.11 Microwave measurements of the 5×5 μm ² device	69
5.12 Comparison of extracted capacitor impedance and simulated impedance for 5×5 μm ² device	70
5.13 Temperature dependence of S11 for varactor on sapphire at 0V	72
5.14 Temperature dependence of S21 for varactor on sapphire at 0V	72
5.15 Temperature dependence of S11 for varactor on sapphire at 2V	73
5.16 Temperature dependence of S21 for varactor on sapphire at 2V	73
5.17 Voltage dependent dielectric constant of Ba _{0.6} Sr _{0.4} TiO ₃	74
5.18 Voltage dependent loss tangent of Ba _{0.6} Sr _{0.4} TiO ₃	75
5.19 Temperature dependent dielectric constant of Ba _{0.6} Sr _{0.4} TiO ₃ at 0V	76
5.20 Temperature dependent dielectric loss of Ba _{0.6} Sr _{0.4} TiO ₃ at 0V	76

CHAPTER 1

INTRODUCTION

1.1 Ferroelectric materials

1.1.1 Overview of ferroelectrics

Ferroelectric materials are featured with spontaneous polarization that can be switched by external electric fields. First observed in the Rochelle Salt [1], ferroelectricity has been found to exist in over three thousand types of natural and man-made compounds. Since the early 1940s with the discovery of the phenomenon of ferroelectricity in ceramic barium titanate capacitors due to the unusually high dielectric constant, they have been contributing to several multibillion dollar industries, such as for capacitors in memory. Barium titanate and lead zirconate titanate have dominated the field as the two main compositional systems [2].

1.1.2 Origin of ferroelectrics

Ferroelectricity arises from asymmetry of lattice structure in crystals. Ferroelectric materials are a class of ionic, insulating materials whose low crystal symmetry permits them to have a stable net electric dipole in a certain direction.

Ferroelectrics contain one or more polar axes along which the spontaneous polarization can be developed [3]. The twenty one out of thirty two crystal classes show a pyroelectric effect and exhibit a finite value of polarization (spontaneous polarization) in the absence of an applied electric field or stress while the rest of the eleven crystal classes are centro-symmetric, they cannot exhibit ferroelectricity. The key property of ferroelectrics is that the direction of spontaneous polarization can be changed by an applied electric field. The ability of ferroelectrics to change their atomic structure under the application of an electric field gives rise to extremely high values of relative permittivity, or dielectric constant. This is one reason ferroelectric materials have attracted much interest in their promising potential for a number of technological applications. The pyroelectric effect in these materials can be used for uncooled infrared radiation detection. Primarily, the properties of switchable non-zero spontaneous polarization find application in Ferroelectric Random Access Memories (FeRAMs). The two stable states in the hysteresis loop correspond to the two binary states "0" and "1".

1.1.3 Applications of ferroelectrics

The applications for ferroelectric ceramics are numerous and pervasive. By far, more research and the largest number of applications in ferroelectrics are still associated with bulk materials, but a trend toward thin films has been steadily increasing. Besides the obvious advantages such as smaller size, lighter weight, and easier integration, FE thin films offer additional benefits including the

following points (1) lower operating voltage (2) higher speed, and (3) unique sub micro level structures.

A number of application areas for FE thin films include (1) non volatile memories (2) capacitors (3) dielectric buffer layers (4) piezoelectric resonators (5) integrated optics switches, couplers and modulators (6) pyroelectric sensors (7) electro-optic displays, and (8) electro-optic, transverse-mode shutter.

1.1.4 Barium Strontium Titanate

Barium strontium titanate ($\text{Ba}_{1-x}\text{Sr}_x\text{TiO}_3$, abbreviated as BST) is a solid solution of barium titanate (BaTiO_3 or BTO) and strontium titanate (SrTiO_3 or STO) and it can be formed over the entire range of concentration x . While BaTiO_3 and SrTiO_3 are two simple-perovskite oxides, BST is usually called a complex perovskite oxide because both Ba^{2+} and Sr^{2+} occupy the A-site in the ABO_3 -crystal structure.

The study of BST thin film is mainly motivated by the potential applications for producing a number of microelectronic components and devices, including infrared sensors and thermal imagers, dynamic random access memory and tunable microwave devices [5]. For applications in tunable microwave devices, the BST thin film is required to exhibit a dc voltage tunable dielectric constant and small loss tangent; thus it is usually employed in paraelectric state, rather than ferroelectric state. So the modifiability of ferroelectric and dielectric properties of BST is the key reason that makes BST useful for so many different applications.

1.2 Electrical properties of ferroelectric material

When integrating these functional ferroelectric materials into design and fabrication of tunable microwave devices, we need to investigate some of the electrical properties of the ferroelectric materials such as polarization vs. electric field (P-E), capacitance vs. voltage (C-V), direct current vs. voltage (I-V). From these quantities, we can derive the dielectric properties of the material which are important for circuit design.

1.2.1 Hysteresis loop

Electrical hysteresis typically occurs in ferroelectric material, where domains of polarization contribute to the total polarization. Polarization is the electrical dipole moment (either $\text{C}\cdot\text{m}^{-2}$ or $\text{C}\cdot\text{m}$), which is used to measure the polarity of a system of electric charges. The ferroelectric hysteresis measurement is defined by Radiant Technologies as a "large signal" measurement of the polarization properties of the sample [6] [7]. "Large signal" means that the test waveform has large enough amplitude to switch dipoles in the ferroelectric material. This "large signal" measurement captures every electron that moves into or out of the capacitor and integrates all changes the sample experiences during the test waveform, showing its entire trajectory. The measurement results contain contributions from all components of the sample, including the remnant polarization and parasitics.

1.2.2 Permittivity – electric field ($\epsilon - V$ or $C - V$) relationship

Compared with hysteresis loop measurement, C-V measurement is a small signal capacitance measurement, which is defined as one where the test amplitude is small compared to that required to switch remnant polarization in a ferroelectric capacitor. Since the response of a non-linear sample changes with the absolute value of the voltage applied and the remnant polarization state, the “small signal” measurement must also have a steady state voltage component as well as a remnant polarization pre-set procedure to put the sample in the appropriate state. Therefore, the “small signal” measurement captures and integrates only those changes the sample experiences during a small amplitude simulation of the sample at a specified voltage and polarization state. By definition, the “small signal” measurement contains no contribution from switching dipoles.

1.2.3 Current vs voltage (I-V)

An I/V measurement performs a series of leakage current measurements as voltage is stepped from point to point along a voltage profile. I-V curve can be used to investigate the conduction mechanism of the thin film. For example, examination shows that the most probable mechanisms controlling the nonlinear dc current through perovskite films are: Schottky emission, Pool-Frenkel emission, and space charge limited current (SCLC).

1.3 Microwave applications of ferroelectric materials

Ferroelectrics have been studied since the early 1960s for application in microwave devices [8]. However, only recently applications begin to emerge. The renewed interest is due to a number of factors, one being their compatibility with high-temperature superconductors in terms of their final application and similar methods of production. The tunability in dielectric constant as a function of electric field is the key to a wide range of applications [9].

1.3.1 Review of ferroelectric microwave applications

Examples of applications in the field of microwave engineering include field-dependent varactors, tunable resonators, phase shifters, frequency-agile filters, variable-power dividers and variable-frequency oscillators [4]. Non-linear applications such as harmonic generation, pulse shaping, mixing and parametric amplification are also a possibility. Such components have a wide range of applications in many communication and radar systems. For example, variable-phase shifters, one of the first and simplest components to be made with ferroelectrics, are used in antenna arrays in order to produce a beam scanning function [10]. It is also promising to integrate ferroelectric materials to produce complex electronically steerable antenna arrays with applications in both military and commercial radar and communication systems. Electronically controlled filters can be produced with applications of interference suppression, secure

communications, dynamic channel allocation, signal jamming and satellite and ground-based communications switching. Many new systems concepts will appear as high-performance materials emerge and these systems will have considerably improved performance over conventional systems. Ferroelectric devices are fast, small and lightweight and, because they work using an electric field, have low power consumption. The range of tuning is quite large and devices are relatively simple in nature. Also the ferroelectric components are of small size because the high dielectric constants are involved. The most attractive material is BST films in the context that the complexity of achieving low temperature and the cost of the cryogenic plants necessitated the development of ferroelectric thin film materials with operating temperatures close to room temperature. BST films were found to exhibit an excellent tunable behavior even at room temperature (in the case of 40-60% concentration of barium), which lay the foundation for the microwave tunable devices [10].

In recent years, ferroelectric materials are applied in many advanced microwave circuit designs, like phase shifter, filters etc. Yong-Hoon Chun etc reported a newly developed BST-varactor tunable bandpass filter (BPF) by adopting a novel tunable circuit based on tunable impedance transmission line [11]. Guru Subramanyam et al. had demonstrated a cascaded shunt switch can be used for phase control circuits, which resulted in a differential phase shift of 110 degrees \pm 10 degrees over the bandwidth of 20 and 31 GHz [12]. Fu et al. also presented a coplanar phase shifter based on ferroelectric thin films [13]. Vincent

Laur et al. used $\text{KTa}_{1-x}\text{Nb}_x\text{O}_3$ (KTN) material to fabricate microwave circuits constituted by interdigital capacitors (IDCs) and stubs. They studied topologies of stubs loaded to achieve the desired function of tunable filter [14]. Buslov et al. have designed microwave phase-shifter based on the slot-line. The phase shifter tested served as a basis for the 8-elements phase array antenna, whose scanning sector was 60 deg and beam width was 13 deg [15]. Buslov et al also made a novel design of microwave four-pole band-pass filter based on the tunable waveguide dielectric resonators with the embedded planar $(\text{Ba,Sr})\text{TiO}_3$ film ferroelectric varactors. The bandwidth at 1dB level is about 350 MHz (1.2%), the range of tuning is 570 MHz (1.9%) and insertion losses are no more than 5.0 dB [16]. In the area of ferroelectric varactor, Guru Subramanyam et al. developed a ferroelectric varactor switch which can be useful for microwave/millimeter wave switching as well as for the design of reconfigurable circuits. Experimental performance of the varactor shunt switch indicates good switching performance with 24 dB isolation @ 41 GHz and insertion loss below 7 dB up to 45 GHz [17]. Kim et al presented comparative characteristics of microwave variable capacitors (varactors) fabricated on $\text{Na}_{0.5}\text{K}_{0.5}\text{NbO}_3$ (NKN), $\text{AgTa}_{0.5}\text{Nb}_{0.5}\text{O}_3$ (ATN) and $\text{Ba}_{0.5}\text{Sr}_{0.5}\text{TiO}_3$ (BST) ferroelectric films sintered by pulsed laser deposition technique. The frequency dispersion of capacitance was 37%, 4.3%, and 17%, the voltage tunability (200KV/cm) 22%, 4.7% and 22% at 20 GHz, loss tangent similar to 0.23, 0.068 and 0.137 at 20 GHz for NKN/Nd: YAlO_3 , ATN/ Al_2O_3 , and BST/ Al_2O_3 films capacitors respectively [18]. Besides filter, resonator and varactor mentioned above, a voltage-controlled oscillator

(VCO) is studied by Jamil et al. VCOs are integral parts of phase locked loops, clock recovery circuits and frequency synthesizers and thus are widely used in both discrete and on-chip applications. Ferroelectric varactors are capable of out-performing solid state varactors at microwave frequencies, due to their lower parasitic series resistance that leads to a higher Q-factor [19].

1.3.2 Frequency tunable antenna

Tunable antenna was closely related to thin-film ferrite technology, which contribute to a new class of antennas. The permeability variation of a ferrite substrate with an axial dc magnetic field made possible the tuning of a patch antenna on such a substrate. The development of magnetic tuning of a microstrip patch on a ferrite substrate is presented by Rainville et al. [20]. The authors demonstrated the application of a small in-plane magnetic field to tune the frequency and phase of the radiating field. Radiation characteristics of microstrip antenna biased on ferrite substrate is presented by Pozar [21]. The possibility of sweeping the resonant frequency of a rectangular microstrip antenna on a ferrite substrate was reported by Misra et al. [22], and bandwidth and radiation characteristics of such tunable antennas were measured and compared in the low-frequency range by Das et al [23]. However, all such tuning and integration of circuits and antennas are mainly on ferrite substrate due to magnetic tuning.

With the development of ferroelectric materials, a few groups have been investigating the tunable antenna based on ferroelectric thin film. For example, Jose et al. have reported the frequency tunability of a microstrip antenna achieved on a barium strontium titanate (BST) substrate. A microstrip patch antenna is printed on the tunable dielectric substrate, and the radiation performance was studied for different bias conditions. The antenna frequency can be changed by varying the applied dc voltage [24]. Teo et al. also reported that multi-layered antenna configuration was adopted to solve the problem which is the energy loss associated with the excitation of surface waves modes [25].

Recent years, some groups also report the tunable antennas based on RF MEMS switches and MEMS tunable capacitors designed to control the resonant frequency, bandwidth, polarization, and radiation pattern of these antennas [26] [27] [28]. Emre Erdil et al present a novel tunable frequency microstrip patch antenna using the RF MEMS technology. The structure consists of a patch antenna loaded with a coplanar waveguide (CPW) loading section attached to the antenna via microstrip to CPW transition. The reconfigurability in the resonant frequency of the antenna is provided with the aid of the MEMS bridges acting as variable capacitors placed on the CPW stub [29].

1.4 Objective of the study

Research is conducted to develop an electrical property characterization system both for the low frequency and microwave frequency range. Meanwhile, it is

desired to seek prospective functional materials for applications. Based on the varactor shunt switch developed by Guru Subramanyam, it is crucial to further investigate its electrical properties such as temperature dependent scattering parameters, frequency dependent impedances in order to facilitate integration with other electrical components, such as a sensor, antenna, RF amplifier etc. For the energy harvesting purpose, it is planned to design the RF to DC antenna rectifier to make use of randomly distributed microwave energy at certain frequency range.

1.5 Significance of the study

We developed a complete experimental setup for electrical property characterization techniques covering a wide frequency spectrum. The research demonstrates the feasibility of a rapid bio-enabled approach to form ferroelectric BaTiO₃ at room temperature from an aqueous salt solution at near neutral pH. Our research develops a rectifying antenna with a resonant frequency of 2.45 GHz. Also our research initiated the development of tunable frequency antenna by integrating the varactor shunt switch. The investigation on temperature dependent scattering parameters and frequency dependent impedances contribute to the further the integration of varactor shunt switches in microwave circuits.

1.6 Organization of the thesis

Chapter 1 introduces the ferroelectrics, antenna rectifier and tunable frequency antenna

Chapter 2 develops the electrical property characterization techniques and proposes the experimental setup

Chapter 3 presents the RF antenna rectifier circuit design and experimental results

Chapter 4 initiates the tunable frequency antenna design

Chapter 5 gives the experimental characterization results obtained on ferroelectric thin films, and varactor devices.

Chapter 6 summarizes the thesis and provides outline of future work

CHAPTER 2

ELECTRICAL CHARACTERIZATION TECHNIQUES AND EXPERIMENTAL SETUP

2.1 Introduction to electrical characterization techniques

With the trend of novel electronic material development, it is of great necessity to know the important electrical properties which will better serve the processing and design of those materials. In our group's research on developing a novel RF varactor shunt switch, we found that the task of how to accurately characterize the electrical properties for those functional materials over a broad frequency range is crucial for the device fabrication and design. Electrical characterization techniques include both low frequency ($< 1\text{MHz}$) and microwave frequency ($> 1\text{GHz}$) measurement. We use a Radiant Technologies Precision LC Tester to measure the low frequency properties and a Vector Network Analyzer (VNA) to characterize the microwave properties. For low frequency, there are three main electrical curves we are targeting: Hysteresis Loop (Polarization vs. Applied electric Field), C-V curve (Capacitance vs. Voltage), I-V curve (Leakage Current vs. Voltage), which can be obtained through Radiant Tester. Microwave characterization is performed using the varactor capacitive

test structure from the scattering parameters obtained from VNA to derive the dielectric properties in the microwave frequency range. Both low and high frequency measurements can be integrated into one characterization system, which enables determining properties over a wide spectrum.

2.2 Electrical properties characterization system

In our lab, the electrical properties characterization system has been setup as shown in Figure 2.1 and Figure 2.2 for the hardware part. The integral system can implement the characterization over the whole spectrum. Either Radiant LC tester or vector network analyzer is linked to the probe station to implement low frequency or microwave frequency measurement. The on-wafer measurements are carried out using the probe station. Both the systems are connected to a single computer through General Purpose Interface Bus (GPIB) to achieve automatic data acquisition. Thermoelectric temperature controller can be used to investigate the temperature dependent electrical properties especially for pyroelectric materials. Besides the hardware, Vision software is used for low frequency characterization while Microwave Office is employed for microwave frequency characterization.

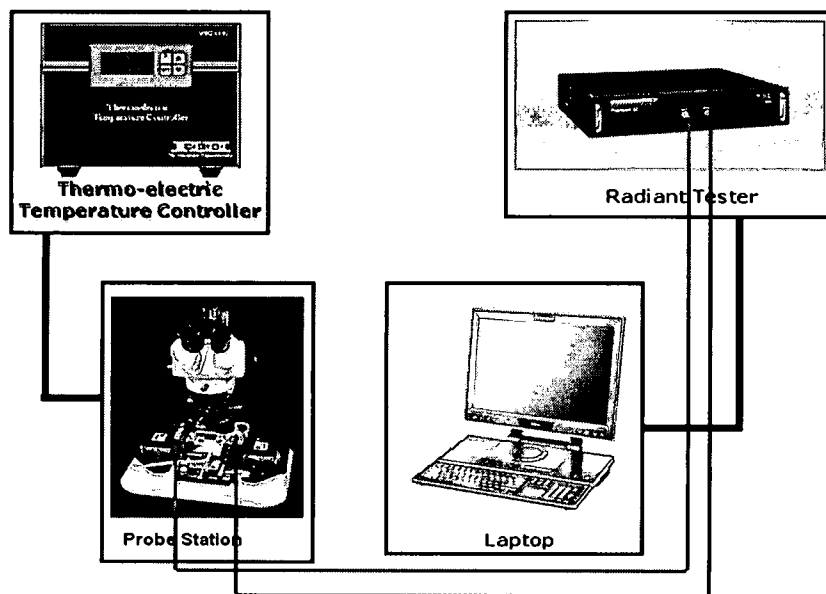


Fig.2.1 Low frequency characterization system setup

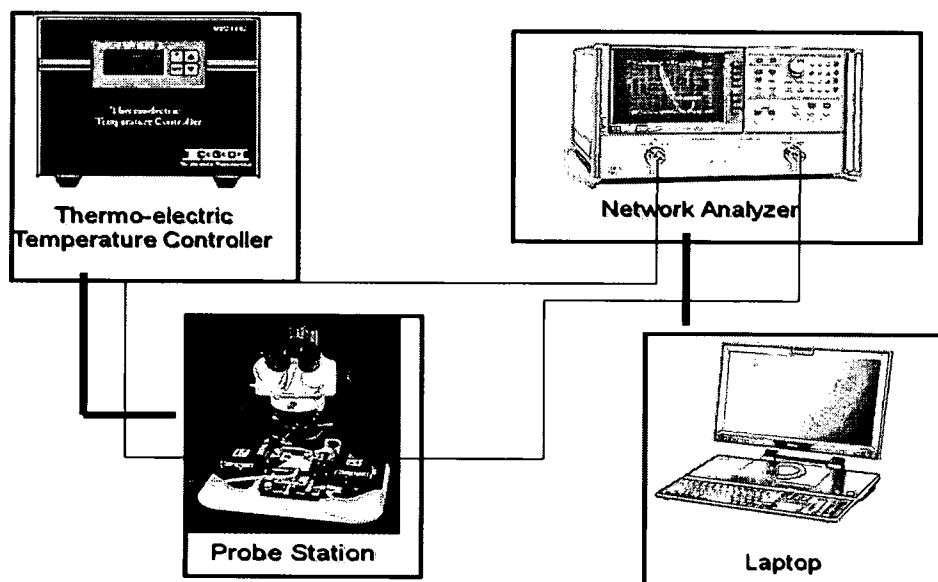


Fig.2.2 Microwave frequency characterization system setup

2.3 Samples

There are different kinds of samples we are interested in investigating: standard packaged discrete capacitors and wafer based thin films and bulk electronic materials.

2.3.1 Standard capacitors

The samples are ferroelectric materials which are packaged into a standard TO-18 package. Such capacitors can be easily connected through the Radiant Socket Board, which is laid out in a way to preserve shielding of the signal lines and preserve the noise limiting effect of the coax cables attaching the socket board to the ferroelectric tester as well as the shielding provided by the case connection of the TO-18 can. Even if the samples are not adequate to use the Radiant Socket Board, the material can be processed into the standard packaged thin film capacitors so that they can be fit for the socket board.

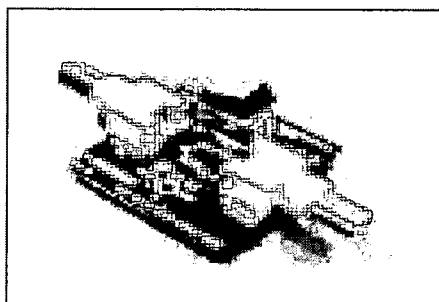


Fig.2.3 Radiant socket board

2.3.2 Wafer based samples

The samples are made of novel material deposited on the certain type of wafers, like high resistivity silicon, and sapphire. The probe station and special probes are required during the measurement. DC probes are used for low frequency on-wafer measurements and Ground-Signal-Ground coplanar probes are used for on-wafer microwave measurements.

2.3.3 Bulk materials

Since the single Radiant LC tester is exclusively used for thin film measurement, the bulk samples measurement can only be executed with the aid of high voltage equipment and high voltage test fixture. The high voltage equipment can allow the Precision test system line to execute tests at voltages up to 10,000 V and also provide protection to the user from the high voltages present during tests. The high voltage test fixture is a unique Teflon sample holder for bulk ceramic devices. This sample holder is rated to 200-230°C and can be used with silicon oil to apply heat within all chambers.

2.4 Low frequency measurement (< 1MHz)

Low frequency measurement is performed through Radiant Tester, which is capable of executing a variety of tasks including hysteresis loop measurement, small signal CV, IV, leakage current, remnant hysteresis, fatigue, imprint,

retention, voltage breakdown, piezoelectric displacement, and others. Along with the hardware, Vision Software is served as a virtual tester which can construct complex programs with any number of tests to characterize all aspects of the sample in one execution while keeping track of the measurement results and the history of the sample being tested.

2.4.1 Hysteresis loop

The hysteresis Loop is the curve of polarization vs. applied electric field. Sawyer and Tower first discovered the hysteresis loop in Rochelle salt based on circuit in Fig 2.4 [30].

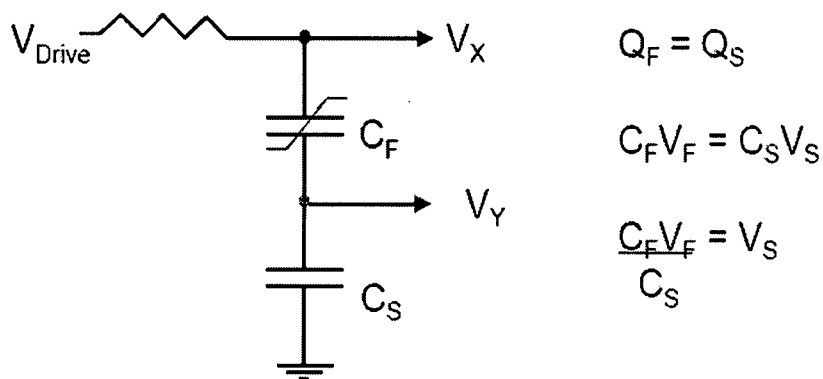


Fig.2.4 Sawyer tower circuit

From Fig.2.4, by measuring the potential V across a standard capacitor in series with the ferroelectric material one can determine the charge on the FE capacitor using $Q=CV$. When two capacitors are in series the charge on each capacitor must be the same (in an ideal capacitive circuit no current flows), so the electric charges on the standard capacitor and the FE capacitor are the same. As the

capacitance C of the standard capacitor is known we are able to calculate Q from the magnitude of the voltage signal we measure at the standard capacitor [19].

Fig.2.5 illustrates the simple experimental setup of Sawyer Tower circuit.

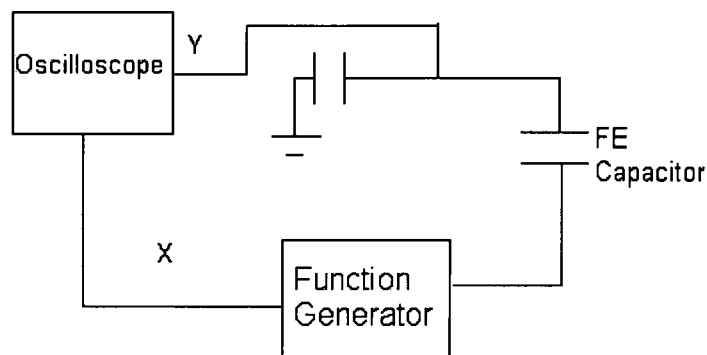


Fig.2.5 A simple experimental setup for hysteresis loop measurement

The ferroelectric hysteresis measurement is defined as a “large signal” measurement of the polarization properties of the sample. This “large signal” measurement captures every electron that moves into or out of the capacitor and integrates all changes the sample experiences during the test waveform, showing its entire trajectory. The measurement result contains contributions from all components of the sample, including the remnant polarization and parasitics. Fig 2.6 shows the interface of hysteresis loop measurement in the Vision software. Usually there are four parameter values required to enter: V_{Max} , area of the capacitor, thickness of the capacitor and hysteresis period, which are all indicated in the figure below. Other values are default. Drive profile type can be changed by creating our own. The critical parameter determining the hysteresis curve is the hysteresis period, which normally ranges from 0.1 ms to 1000 ms.

Hysteresis Setup

Hysteresis Task Name: Hyst-2

VMax: 5 Hyst Offset: 0

Area (cm²): 0.0001 Thickness (μm): 0.3 Hysteresis Period (ms): 10 Pre-Loop Delay (ms): 1000

☐ Adjust Parameters in a Loop

Drive Profile Type: Standard Bipolar
From File
Standard Monopole

Sample Name (24 Characters Max.): _____ Lot ID (12 Characters Max.): _____
Wafer ID (12 Characters Max.): _____

Die Row: 0 Die Column: 0 Capacitor Number: 0

Multi-Channel Options

Sensor Enable	Sensor Scale	Sensor Offset	Sensor Label	Sensor Impedance
<input type="checkbox"/>	<u>1</u>	<u>0</u>		<u>50</u>

Sensor Data = $\text{Sensed Voltage} \cdot ((\text{Input Impedance} + \text{Sensor Impedance}) / \text{Input Impedance}) \cdot \text{Scale} + \text{Offset}$

Comments (255 Characters Max.): _____

☐ Internal Amplifier ±100.0 Volts
☐ External Amplifier
☐ +/- 500 V
☐ +/- 2000 V
☐ +/- 4000 V
☐ +/- 10000 V
☐ Custom Amp

HVI Comm Port: 0 HVI Channel: 0

☐ Drive Channel: 0 ☐ Return Channel: 0
☐ Drive Port: 0 ☐ Return Port: 0

☐ Adjust Mux in a Loop
☐ Enable Ref. Cap. 1nF ±0.1% (Max = 30 Volts)
☐ Enable Ref. Resistor 2.5 M-Ohm ±0.1% (Max = 100 Volts)

☒ Drive Closed
☒ Return Closed
☐ Enable Centering

Amp. Level: 100.0
10.0
1.0
0.1
0.01
0.001
0.0001
0.00002
0.000002
0.0000002

☒ Preset Loop
☒ Start with Last Amp Value
☒ Auto Amplification

Help OK Cancel/Plot

Hysteresis Version: 3.1.1 - Radiant Technologies, Inc., 2000 - 12/12/05

RADIANT TECHNOLOGIES, INC. **PERROELECTRIC TEST SYSTEMS**

Fig.2.6 Demonstration of hysteresis loop setup

2.4.2 C-V measurement

C-V curve is a direct indicator of capacitance tunability. Compared with hysteresis loop measurement, C-V measurement is a small signal capacitance measurement, which is defined as one where the test amplitude is small compared to that required to switch remnant polarization in a ferroelectric capacitor. Since the response of a non-linear sample changes with the absolute value of the voltage applied and the remnant polarization in a ferroelectric capacitor. The "small signal" measurement must also have a steady state

voltage component as well as a remnant polarization pre-set procedure to force the sample in the appropriate state. Therefore, the “small signal” measurement captures the changes the sample experiences during a small amplitude stimulation of the sample at a specified voltage and polarization state. By definition, the “small signal” measurement contains no contribution from switching dipoles.

The screenshot shows the 'Advanced C/V Configuration' dialog box with the 'Profile Setup' tab selected. The 'C/V Task Name' is 'Adv C/V-1'. The 'Area (cm²)' is 0.0001 and 'Thickness (nm)' is 0.3. The 'Voltage Range' is set to 'Internal Amplifier' with a range of ±100.0 Volts. The 'HVI Comm Port' is 0 and 'HVI Channel' is 0. The 'External Amplifier' options are: ±500 V, ±2000 V, ±4000 V, ±10000 V, and Custom Amp. The 'Sample Name' (24 Characters Max.) is empty, 'Lot ID' (12 Characters Max.) is empty, and 'Wafer ID' (12 Characters Max.) is empty. The 'Die Row' is 0, 'Die Column' is 0, and 'Capacitor Number' is 0. The 'Drive Channel' is 0, 'Return Channel' is 0, 'Drive Port' is 0, and 'Return Port' is 0. The 'Adjust Mux in a Loop' checkbox is checked. The 'Enable Ref. Cap.' checkbox is checked, with a value of 1nF ±0.1% (Max = 30 Volts). The 'Enable Ref. Resistor' checkbox is checked, with a value of 2.5 M-Ohm ±0.1% (Max = 100 Volts). The 'Drive Closed' checkbox is checked, and the 'Return Closed' checkbox is checked. The 'Multi-Channel Options' section shows 'Sensor Enable' checked, 'Sensor Scale' 1, 'Sensor Offset' 0, 'Sensor Label' 50, and 'Sensor Impedance' 50. The 'Sensor Data' is calculated as 'Sensed Voltage * ((Input Impedance+Sensor Impedance)/Input Impedance) * Scale + Offset'. The 'Start at Last Amp Level' checkbox is checked, and the 'Auto Amplification' checkbox is checked. The 'Comments' (255 Characters Max.) field is empty. The 'Amp. Level' list shows values: 10.0000, 0.5001, 0.0172, 0.0017, 0.0002, HVI - 0.00002, and HVI - 0.000002. The 'Advanced C/V Version' is 3.1.2 - Radiant Technologies, Inc., 2001 - 12/12/05. The 'RADIANT' logo and 'FERROELECTRIC TEST SYSTEMS' are displayed. The 'Help' button is visible. The 'OK', 'Cancel', and 'Apply' buttons are at the bottom right.

Fig.2.7 Demonstration of C-V measurement sample setup

The C-V measurement also requires two step parameter setups: sample setup and drive profile setup. In the sample setup part, it is required to enter the area

and the thickness of the sample accurately as shown in Fig 2.7. The C-V profile setup is shown in Fig 2.8.

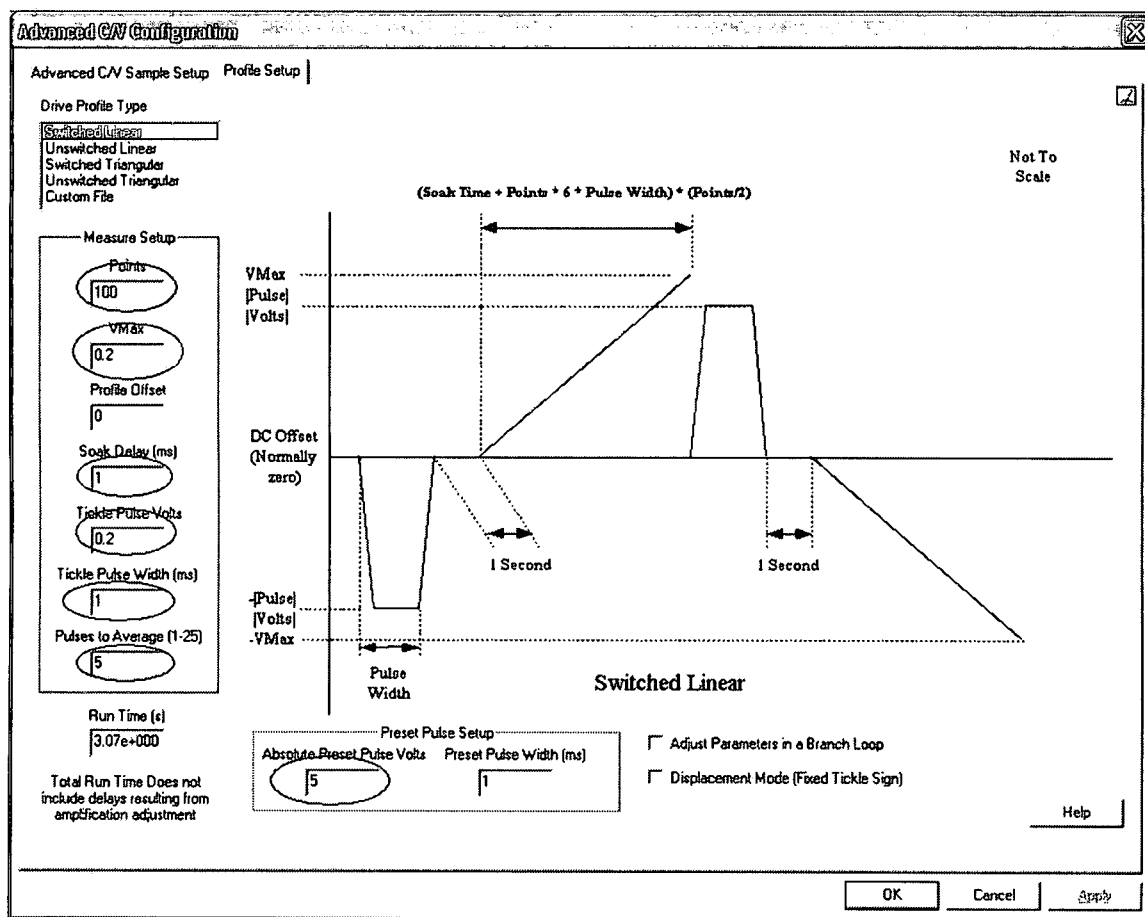


Fig.2.8 Demonstration of C-V measurement drive profile setup

We use the “Switched” type of profile setup for ferroelectric materials. Such kind of profile first features a preset pulse of opposite voltage VMax. The pulse sets the sample into a polarization state that ensures the measurement will switch the sample. Soak delay is a user-controllable duration that occurs before any small signal stimulus is applied to the sample. The purpose of the delay is to allow any current induced by the voltage step to dampen so that the sample is at a steady

state current condition. We can leave at default or increase it as 10ms. Tickle pulse volts is a very critical parameter which is the value of the small signal voltage applied during each stimulus period at each step voltage. The value is normally very small with respect to the step voltage. However, the value can be increased a little bit to prevent the effect of the signal noise and miscellaneous noise. The tickle pulse width is the duration of a single pulse in the small signal measurement of capacitance. It is also the duration between pulses when multiple pulses are used. The value of "pulses to average" is the number of small pulses to be used in making the capacitance measurement at each step voltage. Since the signal applied is very small, the measurement is noise-prone. So increasing this value will reduce the noise in the data. In the preset pulse setup, it is changed equal to or less than the VMax value.

2.4.3 I-V measurement

I-V curve can be used to investigate the conduction mechanism of the thin film. For example, examination shows that the most probable mechanism controlling the non-linear dc current through perovskite films are: Schottky emission, Pool-Frenkel emission, and space charge limited current (SCLC). For electronic material used for chip and device application, it is always desired to keep the leakage current as low as possible so that I-V measurement can contribute to measuring the leakage current flowing through the material.

I-V measurement also requires two step parameter setup: sample setup (shown in Figure 2.9) and profile setup (shown in Figure 2.10). In the sample setup part,

it is required to enter the area and thickness of the sample. Regarding the profile setup, it is more complex due to more parameter values to assign. The default I/V profile is switched linear. "Switched" type of profile is used in order to let the measured sample return to its original state at the beginning of the measurement. Linear profiles require the number of points to be evenly divisible by two. The software will ensure this, regardless of the number of points entered. Triangular profiles also require an even number of points. They have the additional stipulation that the number of points may not be evenly divisible by four. For identical input points, the triangular step size will be twice that of the linear since the triangular waveform must step to VMax and back (or 2 times VMax) in the same number of points. Points are the total number of voltage steps to be taken in the profile. The more points entered results in more voltage steps. "Measure Time" is the duration over which the sample remains at a particular bias voltage. This parameter determines the measurement result very much. If the curve is flat or not correct, we can try to decrease the value of "Measure Time". In the Preset Pulse Setup, one needs to be very careful not to leave the value as 5V which may be too high for some thin films. Normally it is changed equal to the VMax.

I-V Configuration

I/V Main Setup | I/V Profile Setup | I/V Plot Setup

I/V Task Name: I/V-1

Sample Name (24 Characters Max): Thickness (um) 0.3

Lot ID (12 Characters Max):

Wafer ID (12 Characters Max):

Die Row: 0 Die Column: 0 Capacitor Number: 0

Multi-Channel Options:

☐ Sensor Enable

Sensor Slope: 0 Sensor Offset: 0 Sensor Label: 90 Sensor Impedance: 50

Sensor Data = Sensored Voltage * ((Input Impedance + Sensor Impedance) / Input Impedance) * Scale + Offset

Auto Amplification Off is Recommended

Start with Last Amp Level

Auto Amplification

Comments (255 Characters Max):

Errors: Help

I/V Version: 3.1.1 - Radiant Technologies, Inc., 2000 - 10/17/03

RADIANT ELECTRIC TEST SYSTEMS

OK Cancel Stop

Fig.2.9 Demonstration of I-V measurement setup

I-V Configuration

I/V Main Setup | I/V Profile Setup | I/V Plot Setup

I/V Profile

Profile Preview

Not To Scale

Leakage Setup:

VMax: 5

Points: 100

Static

Soak Time (ms): 100

Measure Time (ms): 100

Step Delay (ms): 100

Drive Bias: 0

Total Run Time (s): 2.34 (2.34)

Total Run Time Does not include delays resulting from amplification adjustment

Adjust Parameters in a Branch Loop

Pretest Pulse Setup:

Absolute Pulse Vols: 5

Pulse Width (ms): 1

Diagram:

(Soak Time + Measure Time + Step Delay) * (Points/2 - 1)

VMax [Pulse] [Vols]

DC Offset (Normally zero)

1 Second

1 Second

-Pulse [Vols]

-VMax

Pulse Width

Switched Linear

Help

OK Cancel Stop

Fig.2.10 Demonstration of I-V measurement drive profile setup

2.5 Microwave frequency measurement (> 1 GHz)

Ferroelectric material is attractive for microwave applications due their properties of low loss, dielectric tunability. It is required to develop a simple and convenient method to characterize the ferroelectric thin films to fully utilize the tunable dielectric properties in microwave circuits. In the past, several groups have reported various approaches for characterizations. David Galt et al reported that they fabricated and characterized electrically tunable high temperature superconductor coplanar microstrip resonators. High frequency capacitance and loss information were extracted from the observed resonances and compared with the low frequency [32] [33]. Qingduan Meng et al. proposed a coplanar waveguide (CPW) bandstop filter to characterize ferroelectric thin films. Using the resonant frequency and Q value of the CPW bandstop filter, the dielectric constant (ϵ_r) and the loss tangent ($\tan \delta$) of the ferroelectric thin film were determined by comparing the measured response with simulated results [34]. Ke Wu et al. presented the developed Computer-aided-design (CAD) models for characterization of ferroelectric materials at microwave frequencies. Complex dielectric constant, voltage tunability, and K-factor (a figure of merit for tunable dielectric defined as phase shift in degrees per dB loss) are determined for the ferroelectric materials with a series of BST/ alumina coplanar waveguides (CPWs) and interdigital capacitors (IDCs). Conformal mapping models are employed to co-relate circuit measurements with the BST film intrinsic properties [35].

2.5.1 Capacitive test structure to characterize novel electronic thin films

Compared with the low frequency measurement technique by using Radiant LC tester, microwave frequency characterization requires a coplanar waveguide capacitor pattern. Based on the varactor shunt switch developed by Guru Subramanyam et al. [36][37], a capacitive test structure is proposed for characterization of dielectric properties of electronic thin films [38][39]. Fig 2.11 provides a three dimensional view of the capacitive test structure, which is designed using coplanar waveguide (CPW) transmission lines on a high resistivity Si substrate ($> 6 \text{ k}\Omega$) with a thin SiO_2 isolation layer. CPW line consists of two ground lines, positioned directly above the ground lines in the bottom metal layer, and a signal line, centered between the ground line and perpendicular to the shunt line in the top metal layer overlaps the shunt line in the bottom metal layer. The active region forms a test capacitor. The test structure has a large ground pad capacitor that results from the overlap of the ground lines in the top and bottom metal. The large ground pad capacitor is in series with the test capacitor, resulting in the equivalent capacitance of the test capacitor.

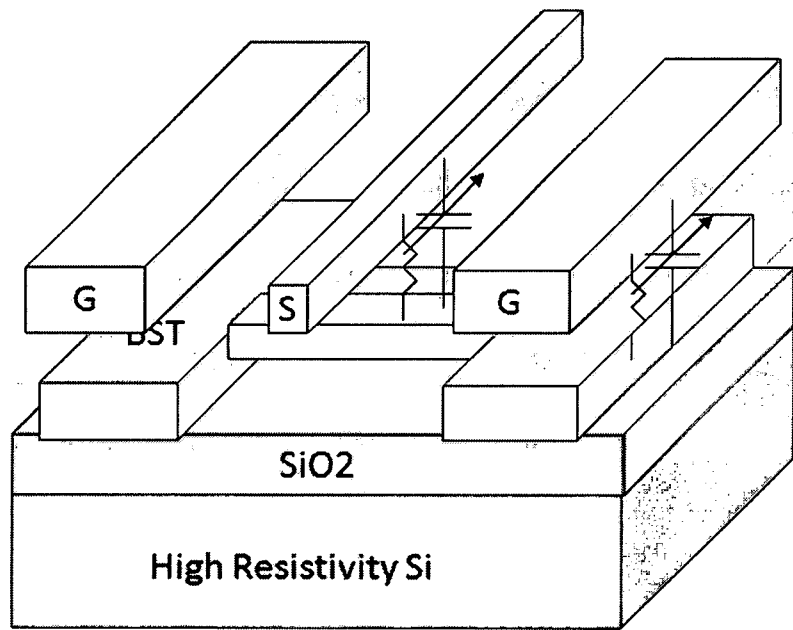


Fig.2.11 Three dimensional view of capacitive test structure

An electrical model of the capacitive test structure is shown in Fig.2.12. In this model, $C(V)$ is the test capacitance of the targeted electronic material in the active region, and $R(V)$ is the shunt resistance modeling leakage conductance of the test capacitor. R_s and L are the parasitic series resistance and inductance for the test capacitor. Employing this electrical model and scattering parameters (S_{11} and S_{21}) measured from the VNA, the relative dielectric constant (ϵ_r) and loss tangent ($\tan \delta$) of the electronic material can be derived through matching the simulation results and experimental results.

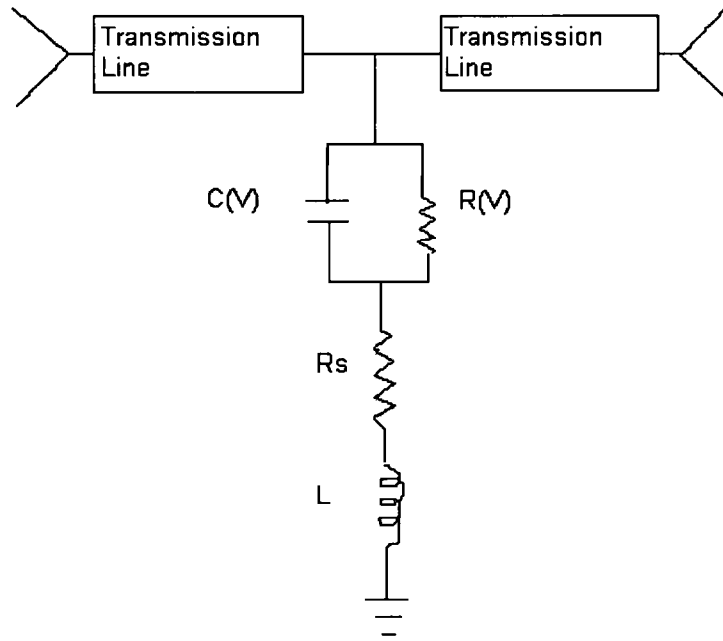


Fig.2.12 The electrical model for the capacitive test structure

From the equation for the capacitance of a parallel plate capacitor, the relative dielectric constant can be computed as

$$\epsilon_r = \frac{C(V)t}{\epsilon_0 A} \quad (2.1)$$

Where $C(V)$ is the capacitance, A is the overlap area of the capacitor and t is the thickness of the material. The loss tangent is derived based on shunt resistance.

$$\tan(\delta) = \frac{1}{\omega R(V)C(V)} \quad (2.2)$$

CHAPTER 3

RF POWER CONVERTER CIRCUIT DESIGN

3.1 Overview of wireless microwave power transmission technology

The concept of wireless power transmission was initiated with the ideas and demonstrations by Tesla [40]. The efforts to promote wireless power transmission started in the 1920's and 1930's. However, the fast development started in the 1950's which was advanced by high-power microwave tubes by Raytheon Company, Waltham, MA [41]. The first receiving device for efficient reception and rectification of microwave power emerged in the early 1960's. A rectifying antenna, namely rectenna was developed, comprised of a half-wave dipole antenna with a balanced bridge or single semiconductor diode placed above a reflecting plane. 2.45 GHz emerged as the transmitting frequency of choice due to its advanced and efficient technology base, location at the center of an industrial scientific, and medical (ISM) band, and its minimal attenuation through the atmosphere even in heavy rainstorms [42].

In the space scale, microwave power transmission can fulfill two major needs for further development of space. One of these needs is large amounts of electric power at reasonable cost for manufacturing operations in low-earth orbit. The other need, an extension of the first, is for large amounts of power for electric

propulsion needed for a greatly improved space transportation system [43]. Also microwave power transmission is the key technology necessary for the future solar power satellites (SPS's) [44]. The electrical power will be generated by solar cells in space and transmitted by microwaves of 2.45 GHz from the SPS to a rectenna site on the ground [45]. In such a way, it can serve as a potential alternative to produce a clean energy source by rectifying the microwave power, especially in some cases when the supply of electricity is not accessible.

In the past, there has been already some research done in the wireless microwave power transmission area. Different kinds of electrical components were designed, where rectenna means "rectifying antenna". The rectenna is a microwave receiver and a converter of microwaves into dc power as the microwave power transmission system. Recently, Y.-J. Ren et al have reported a new rectifying antenna for 35 GHz wireless power transmission [46]. Previously, Jamal Zbitou et al presented a hybrid sensitive rectenna system at 2.45 GHz by achieving a 2×2 patch antenna array, where an RF-dc conversion can be achieved [47].

The general setup for antenna rectifying system used for wireless power transmission is shown in Fig 3.1. It consists of the antenna, rectifying circuit and load [48].

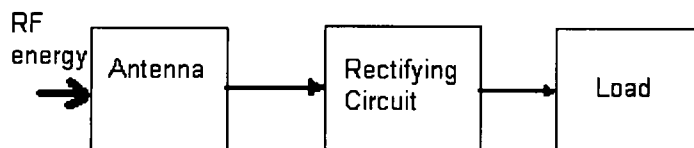


Fig.3.1 Schematic antenna rectifying system

3.2 2.45 GHz patch antenna design

3.2.1 Basic patch antenna design

A planar patch antenna was designed and simulated for a relatively small physical size and appropriate directivity at the desired frequency band, which is normally the ISM radio band. The industrial, scientific and medical radio bands were originally reserved internationally for the use of RF electromagnetic fields for industrial, scientific and medical purposes other than communications. In general, communications equipment must accept any interference generated by ISM equipment. In recent years these bands have been shared by license-free error-tolerant communications applications such as wireless LANs and cordless phones in the 915MHz, 2.45 GHz and 5.8 GHz. Our antenna is designed at 2.45 GHz.

Our patch antenna design is based upon transmission-line model, which represents the microstrip antenna by two slots separated by a low-impedance Z_c transmission line of length L . The effective dielectric constant is defined as the dielectric constant of the uniform dielectric material. The initial value (at low frequencies) of the effective dielectric constant is referred to as the static values, and they are given by equation (3-1) [49]

$W/h > 1$

$$\epsilon_{reff} = \frac{\epsilon_r + 1}{2} + \frac{\epsilon_r - 1}{2} \left[1 + 12 \frac{h}{W} \right]^{-1/2} \quad (3-1)$$

Where W is the width of the antenna, h is the height of the substrate, L is the length of the antenna. ϵ_r is the relative permittivity of the substrate.

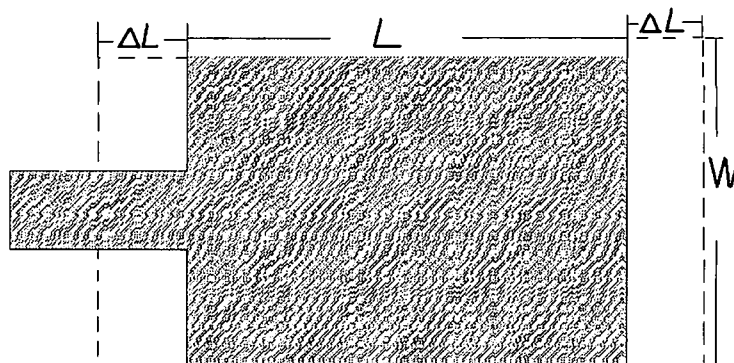


Fig.3.2 Physical and effective lengths of rectangular microstrip patch

Due to the fringing effects, electrically the patch of the microstrip antenna is effectively larger than its physical dimensions. For the principle E-plane (xy-plane), this is shown in Fig 3.2 where the dimensions of the patch along its length have been extended on each end by a distance ΔL , which is a function of the effective dielectric constant ϵ_{eff} and the width-to-height ratio (W/h). A very popular and practical approximate relation for the normalized extension of the length is illustrated in equation (3-2) [50]:

$$\frac{\Delta L}{h} = 0.412 \frac{(\epsilon_{\text{eff}} + 0.3) \left(\frac{W}{h} + 0.264 \right)}{(\epsilon_{\text{eff}} - 0.258) \left(\frac{W}{h} + 0.8 \right)} \quad (3-2)$$

Based on the simplified formulation that has been described, a design procedure is outlined which leads to practical designs of rectangular microstrip antennas. The procedure assumes that the specified information includes the dielectric

constant of the substrate (ϵ_r), the resonant frequency (f_r), and the height of the substrate h . The procedure is stated as follows:

A. For an efficient radiator, a practical width that leads to good radiation efficiencies is calculated in equation (3-3) [51]:

$$W = \frac{1}{2f_r \sqrt{\mu_0 \epsilon_0}} \sqrt{\frac{2}{\epsilon_r + 1}} = \frac{v_0}{2f_r} \sqrt{\frac{2}{\epsilon_r + 1}} \quad (3-3)$$

where v_0 is the free-space velocity of light.

B. Determine the effective dielectric constant of the microstrip antenna using (3-1)

C. Once W is found using (3-2) to determine the extension of the length ΔL (3-2)

D. The actual length of the patch can now be determined by

$$L = \frac{1}{2f_r \sqrt{\epsilon_{eff}} \sqrt{\mu_0 \epsilon_0}} - 2\Delta L \quad (3-4)$$

3.2.2 Patch antenna impedance match to a 50Ω feed line

To connect the antenna to the rectifying circuit, it is expected to design the antenna with the input impedance of 50 Ω.

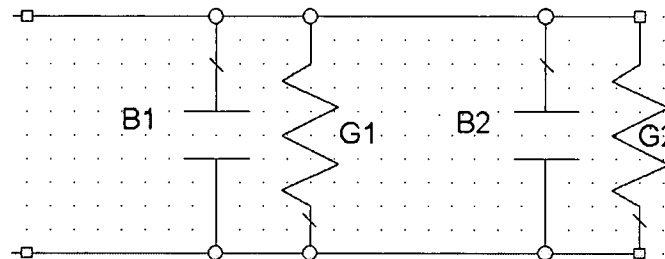


Fig.3.3 Equivalent circuit transmission-line model

From Fig 3.3, the patch antenna has an equivalent circuit transmission-line model. Each radiating slot is represented by a parallel equivalent admittance Y which includes conductance G and susceptance B .

$$Y_1 = G_1 + jB_1 \quad (3-5)$$

Based on the field expression derived by cavity model, the conductance G can be expressed as

$$G_1 = \frac{I_1}{120\pi} \quad (3-6)$$

where

$$I_1 = \int_0^\pi \left[\frac{\sin(\frac{k_0 W}{2} \cos \theta)}{\cos \theta} \right]^2 \sin^3 \theta d\theta \quad (3-7)$$

Ideally the two slots should be separated by $\lambda/2$ where λ is the wavelength in the dielectric. However, the length of the patch is electrically longer than the actual length due to fringing. If the reduction of the length is properly chosen using (3-2) (typically $0.48\lambda < L < 0.49\lambda$) [52][53], the transformed admittance of slot #2 becomes

$$\tilde{Y}_2 = \tilde{G}_2 + j\tilde{B}_2 = G_1 - jB_1 \quad (3-8)$$

So the resonant input impedance is real

$$Z_{in} = \frac{1}{Y_{in}} = \frac{1}{Y_1 + \tilde{Y}_2} = \frac{1}{2G_1} = R_{in} \quad (3-9)$$

Taking the mutual effects into account between the slots, the resonant input impedance can be modified to

$$R_{in} = \frac{1}{2(G_1 \pm G_{12})} \quad (3-10)$$

Where the mutual conductance G_{12} can be calculated as [54],

$$G_{12} = \frac{1}{120\pi^2} \int_0^\pi \left[\frac{\sin(\frac{k_0 W}{2} \cos \theta)}{\cos \theta} \right]^2 J_0(k_0 L \sin \theta) \sin^3 \theta d\theta \quad (3-11)$$

The plus (+) sign is used for modes with odd (anti-symmetric) resonant voltage distribution beneath the path and between the slots while the minus (-) sign is used for modes with even (symmetric) resonant voltage distribution.

It is shown in Fig 3.4 that the resonant input resistance can be changed by using an inset feed, recessed a distance y_0 from slot # 1. W_0 is the width of the microstrip line while y_0 is a distance recessed from slot #1. Considering the inset feed position, the inset-feed input resistance is expressed as [55]

$$R_{in}(y = y_0) = \frac{1}{2(G_1 \pm G_{12})} \cos^2\left(\frac{\pi}{L} y_0\right) = R_{in}(y = 0) \cos^2\left(\frac{\pi}{L} y_0\right) \quad (3-12)$$

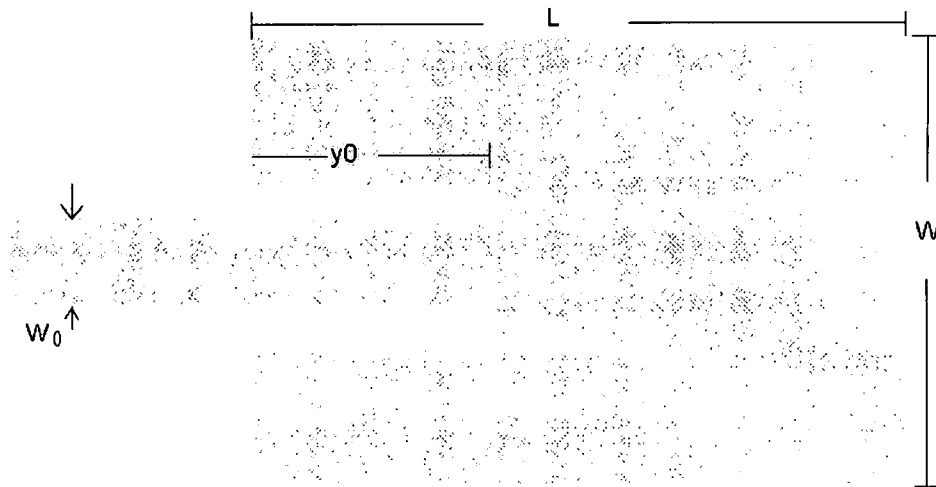


Fig.3.4 Recessed microstrip-line patch antenna

Practically, the gap of the notch has a strong influence on the return loss of the patch antenna. There is a new design approach proposed by Afroz J.Zaman et al [56]. They consider the notch region as a short section of a grounded coplanar waveguide (GCPW) and establish a design rule for the width of the notch, which provides a complementary way to design impedance matching patch antenna.

3.3 Schematic power converter circuit design

Such a kind of rectifier is a combination of an input matching circuit, a shunt output bypass capacitor, a load resistor and a commercial Schottky diode as shown in Figure 3.5.

When the RF signal illuminates the antenna, which serves as the receiving port, it will transfer the microwave power through the waveguide to diode. After rectifying the RF AC signal, there is DC voltage at the output port. From the

schematic, it is crucial to determine the value of shunt capacitor, load resistor, the type of Schottky diode, and the design specifics of matching circuit. Taking the Schottky diode, capacitor and resistor as a whole, the impedance of the three components can be calculated in order to facilitate the matching circuit design.

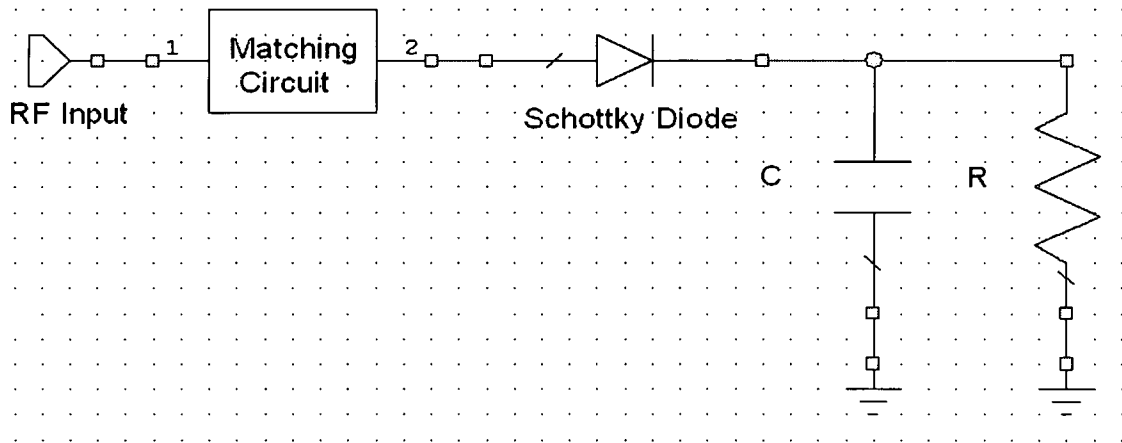


Fig.3.5 Simple antenna rectifying circuit

3.4 Impedance matching circuit design

Based on the previous antenna design and load impedance characterization, there is mismatch between the 50 Ohm impedance of antenna and the impedance of the load. So it is necessary to design the impedance matching layout to maximize the power transfer along the microstrip waveguide.

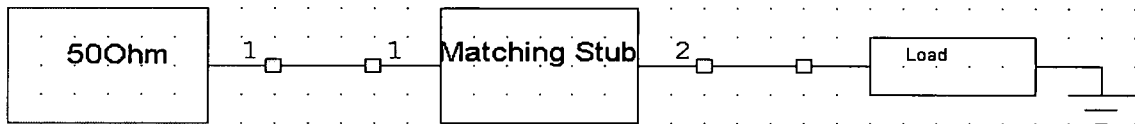


Fig.3.6 Schematic view of microstrip waveguide for rectifying circuit

Normally there are two ways for the impedance matching circuit design. One is matching with lumped elements. Another is stub matching, which uses a single open-circuited or short-circuited length of transmission line (a "stub"), connected either in parallel or in series with the transmission feed line at a certain distance from the load. We choose stub matching method since it is convenient to fabricate in microstrip or stripline form.

In single-stub tuning, the two adjustable parameters are the distance, d , from the load to the stub position, and the value of susceptance or reactance provided by the shunt or series stub, which is represented by the stub length l . For the shunt-stub case, the basic idea is to select d so that the admittance, Y , seen looking into the line at distance d from the load is of the form $Y_0 + jB$. Then the stub susceptance is chosen as $-jB$, resulting in a matched condition. For the series stub case, the distance d is selected so that the impedance, Z , seen looking into the line at a distance from the load, is of the form $Z_0 + jX$. Then the stub reactance is chosen as $-jX$, resulting in a matched condition. We use shunt stub to make the impedance matching as indicated in Figure.3.7 [49].

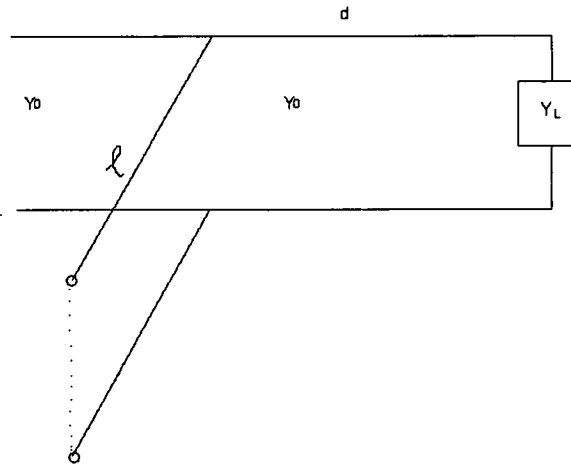


Fig.3.7 Simple-stub matching circuit

To derive formulas for d and l , the load impedance can be written as $Z_L = 1/Y_L = R_L + jX_L$. Then the impedance Z down a length, d , of line from the load is

$$Z = Z_0 \frac{(R_L + jX_L) + jZ_0 t}{Z_0 + j(R_L + jX_L)t} \quad (3-13)$$

Where $t = \tan \beta d$. The admittance at this point is

$$Y = G + jB = \frac{1}{Z} \quad (3-14)$$

Where

$$G = \frac{R_L(1+t^2)}{R_L^2 + (X_L + Z_0 t)^2} \quad (3-15)$$

$$B = \frac{R_L^2 t - (Z_0 - X_L t)(X_L + Z_0 t)}{Z_0 [R_L^2 + (X_L + Z_0 t)^2]} \quad (3-16)$$

Now d (which implies t) is chosen so that $G = Y_0 = 1/Z_0$

So this result in a quadratic equation for t

$$Z_0(R_L - Z_0)t^2 - 2X_L Z_0 t + (R_L Z_0 - R_L^2 - X_L^2) = 0 \quad (3-17)$$

Solving for t gives

$$t = \frac{X_L \pm \sqrt{R_L [(Z_0 - R_L)^2 + X_L^2] / Z_0}}{R_L - Z_0}, \text{ for } R_L \neq Z_0 \quad (3-18)$$

If $R_L = Z_0$, then $t = -X_L / 2Z_0$. Thus the two principle solutions for d are

$$\frac{d}{\lambda} = \begin{cases} \frac{1}{2\pi} \tan^{-1} t, t \geq 0 \\ \frac{1}{2\pi} (\pi + \tan^{-1} t), t < 0 \end{cases} \quad (3-19)$$

To find the required stub lengths, first use t to find the stub susceptance,

$$B_s = -B$$

Then, for an open-circuited stub

$$\frac{l_s}{\lambda} = \frac{1}{2\pi} \tan^{-1} \left(\frac{B_s}{Y_0} \right) = \frac{-1}{2\pi} \tan^{-1} \left(\frac{B}{Y_0} \right) \quad (3-20)$$

If the length above is negative, $\frac{\lambda}{2}$ can be added to give a positive result

For the load including the diode, resistor and capacitor, the normalized load impedance can be simulated.

3.5 Results and measurements

3.5.1 Design of the microstrip patch antenna with matching impedance

The microstrip patch antenna is designed to resonate at 2.45 GHz. From Figure 3.8 shown below, the return loss S11 can reach down to -23dB at the resonant

frequency 2.45GHz, which demonstrates a good antenna design. The designed antenna will be served as the receiving port to harvest the microwave energy at the frequency at 2.45 GHz.

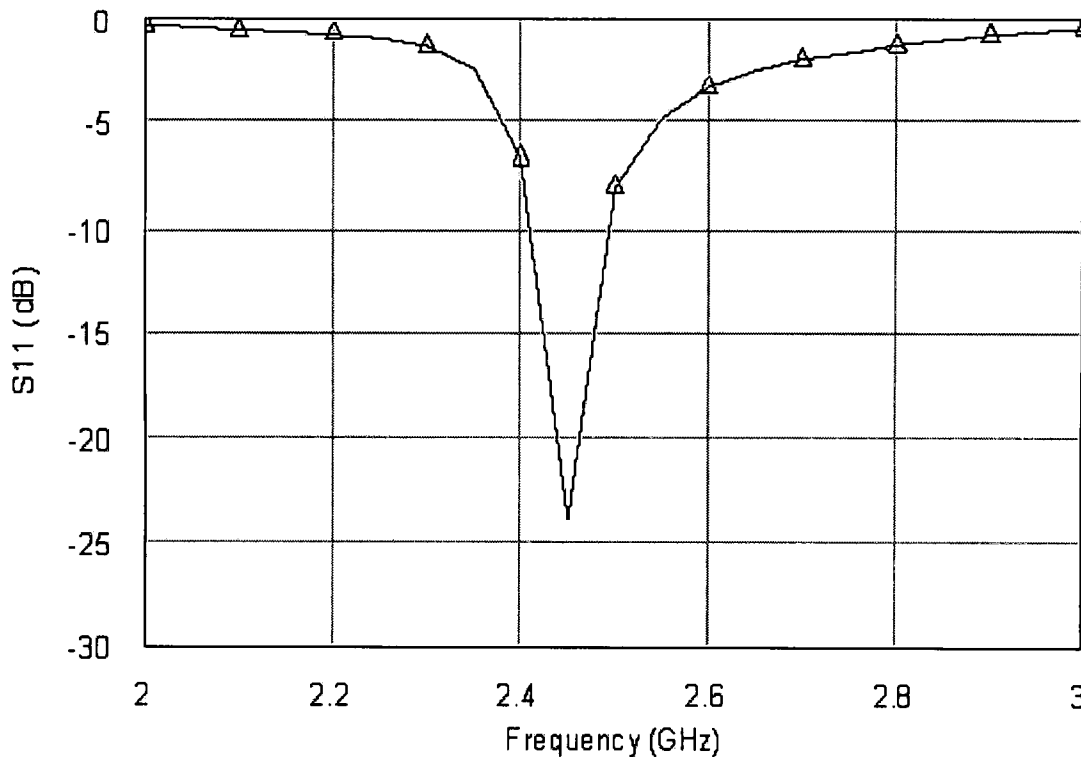


Fig.3.8 Frequency response of return loss S11 for patch antenna

Besides the good S11 return loss performance of the antenna, we want to make sure the impedance of the antenna is the same as the characteristic impedance 50Ω . In this case, the amplitude of the impedance should be 50Ω and the phase angle of the impedance is 0 degrees. Based on the design theory of notch antenna with characteristic impedance, from Fig.3.10 and Fig 3.11 we can see that the impedance amplitude is 50Ω and the impedance phase is approximately 0 degrees, as expected.

The dimension of the designed notch feed antenna is of a rectangular shape of 39.4mm×48.4mm. The notch feed is 48.1mm long. The specifics of the dimensions are shown in Fig 3.9.

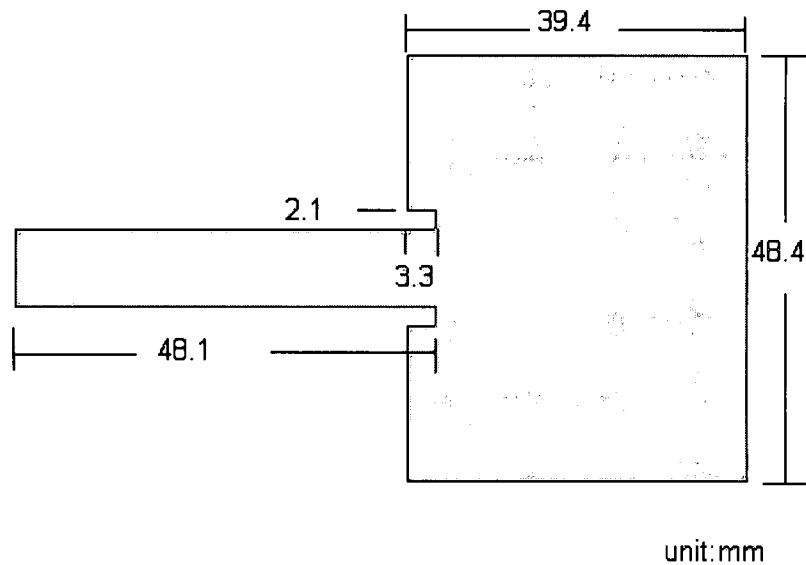


Fig.3.9 Dimensions of designed 2.45 GHz antenna

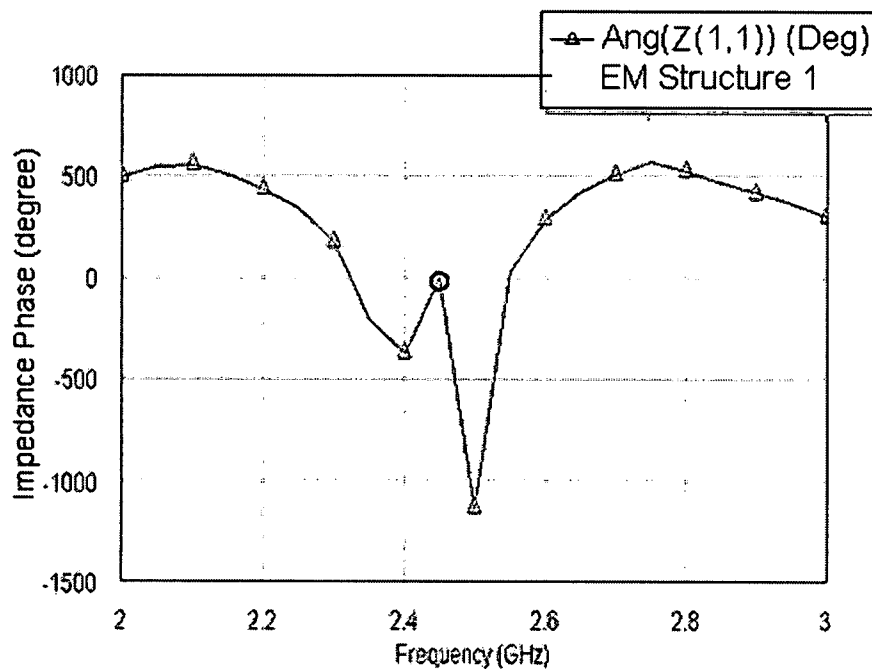


Fig.3.10 Frequency response of impedance amplitude for patch antenna

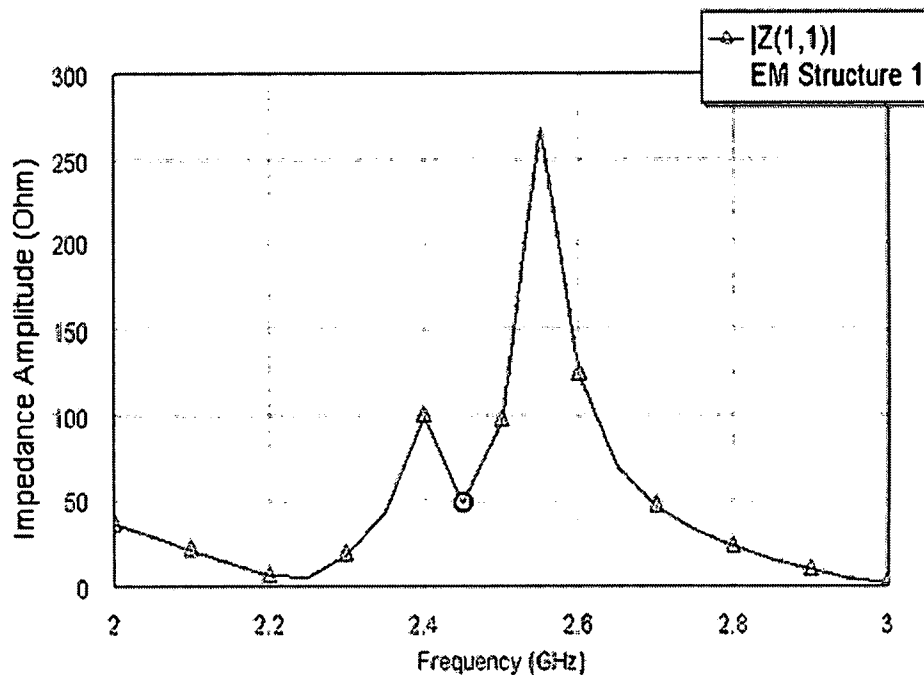


Fig.3.11 Frequency response of impedance phase angle for patch antenna

3.5.2 Diode impedance characterization

In order to minimize the power transfer loss in the circuit, we have to make sure the impedance matching to 50Ω along the electrical components. Therefore, the impedance characterization of the diode should be performed. The diode chip or die itself can be modeled by a three element model as shown in Fig 3.12.

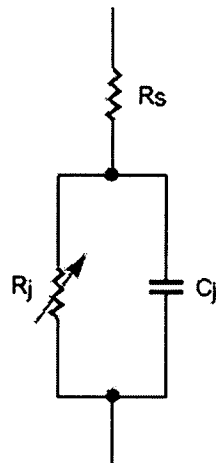


Fig.3.12 Linear model for a diode chip

For the HSMS-2820 diode from Avago Technology we use, it has a package of SOT-23. The three-lead SOT-23 package can be modeled as shown in Fig 3.13, which can provide accurate modeling from DC to 3 GHz.

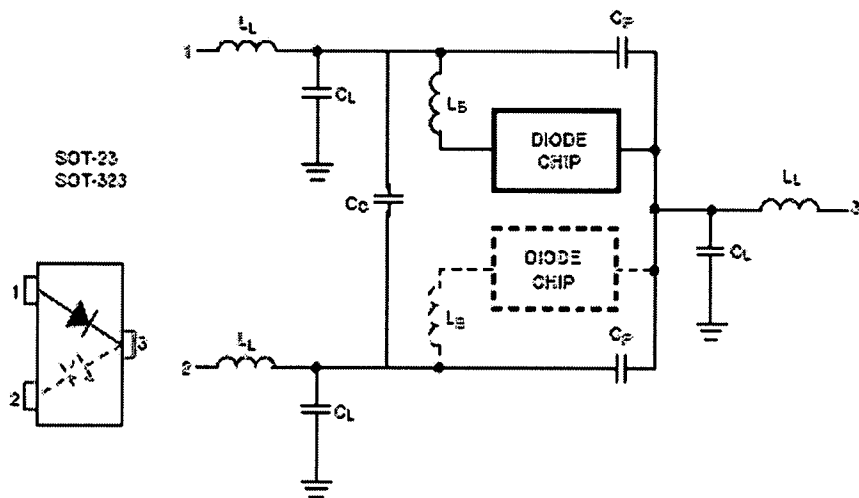


Fig.3.13 Model of the SOT-23 package

We use the microwave office software by simulating the S_{11} parameter to obtain the input impedance of the diode, which is based on the equation below

$$S_{11} = \frac{Z_{in} - Z_0}{Z_{in} + Z_0}$$

So the input impedance can be expressed by

$$Z_{in} = Z_0 \frac{1 + S_{11}}{1 - S_{11}}$$

By including the output resistor and capacitance ($R = 1\text{k}\Omega$, $C = 100\text{pF}$), the impedance of the load is

$$Z_{in} = 25.5347 - 46.7508i$$

3.5.3 Impedance matching microstrip

We use the microstrip waveguide in Figure 3.14 to transfer the microwave energy, which has the characteristic impedance 50Ω .

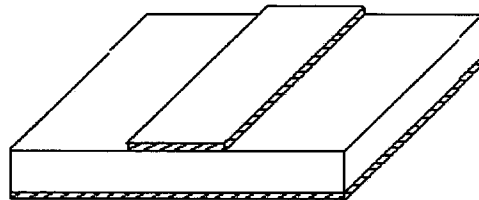


Fig.3.14 Three dimensional view of microstrip waveguide

The screenshot shows the TXLINE 2003 - Microstrip software interface. The top menu bar includes: Microstrip, Stripline, CPW, CPW Ground, Round Coaxial, Slotline, Coupled MSLine, and Coupled Stripline. The main window is divided into several sections:

- Material Parameters:**
 - Dielectric: RT/duroid 5880 (dropdown)
 - Conductor: Copper (dropdown)
 - Dielectric Constant: 2.2
 - Conductivity: 5.88E+07 S/m
 - Loss Tangent: 0.0009
 - AWR logo
- Diagram:** A schematic of a microstrip waveguide on a substrate. It shows a top layer of width W and thickness T , a substrate of height H and dielectric constant ϵ_r , and a ground plane at the bottom.
- Electrical Characteristics:**
 - Impedance: 50 Ohms
 - Frequency: 2.45 GHz
 - Electrical Length: 90 deg
 - Phase Constant: 4062.53 deg/m
 - Effective Diel. Const.: 1.90676
 - Loss: 0.391621 dB/m
- Physical Characteristic:**
 - Physical Length (L): 22.1537 mm
 - Width (W): 9.76399 mm
 - Height (H): 3.175 mm
 - Thickness (T): 0.07 mm

Navigation arrows (back and forward) are located between the Electrical and Physical characteristic sections.

Fig.3.15 Physical characteristics of microstrip waveguide

By using Microwave office TXLINE 2003, it is easy to design the physical characteristics of microstrip waveguide as presented in Figure 3.15. RT/duroid 5880 high frequency laminate from Rogers Corporation is used as the substrate material. The dielectric constant of the RT/duroid 5880 is 2.20 and the dielectric tangent loss is 0.0009. The thickness of the RT/duroid 5880 dielectric is 3.175 mm and 0.07 mm for the copper metal.

3.5.4 Circuit performance as a rectifier

The schematic layout of the antenna rectifier is show in Figure 3.16. The receiving antenna is replaced by a port providing 2.45 GHz RF power.

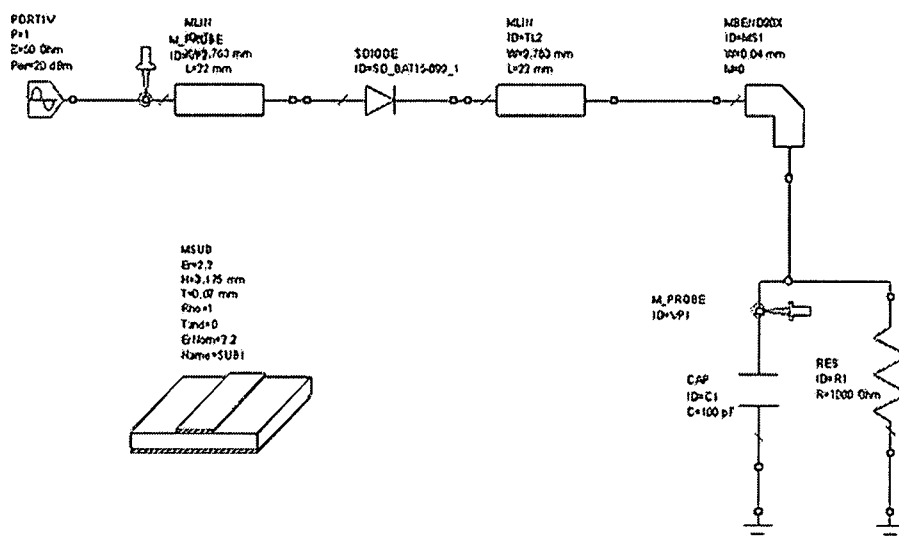


Fig.3.16 Schematic circuit of rectifier antenna

The simulation result of the schematic circuit is in Figure 3.17. The input port provides 20dBm RF power in the form of sinusoidal signal. The output signal is the DC form which comes out of the diode. The value of the output dc signal is around 1.8V. Apart from the layout shown in Figure 3.16, it is also recommended to connect another diode serially with the resistance to level up the output dc voltage. Meantime, the optimization of capacitor and resistor values is necessary to attain the maximum value of the voltage output.

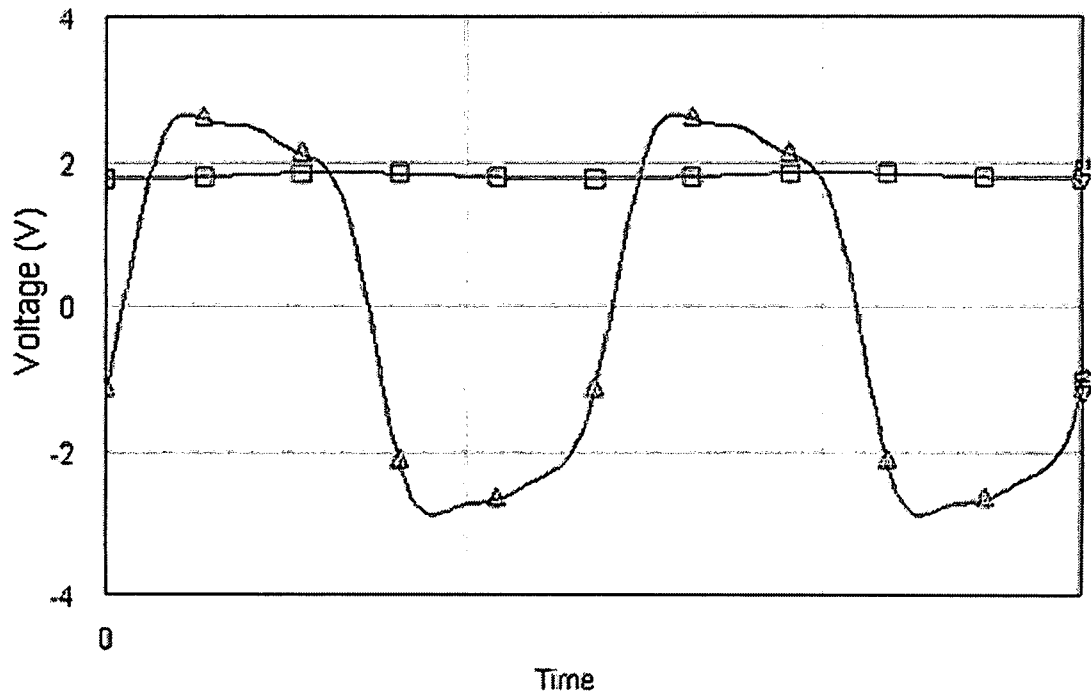


Fig.3.17 Simulation results for schematic equivalent Circuits

Based on the previous calculations, the overall design of antenna rectifier is presented in Fig.3.18.

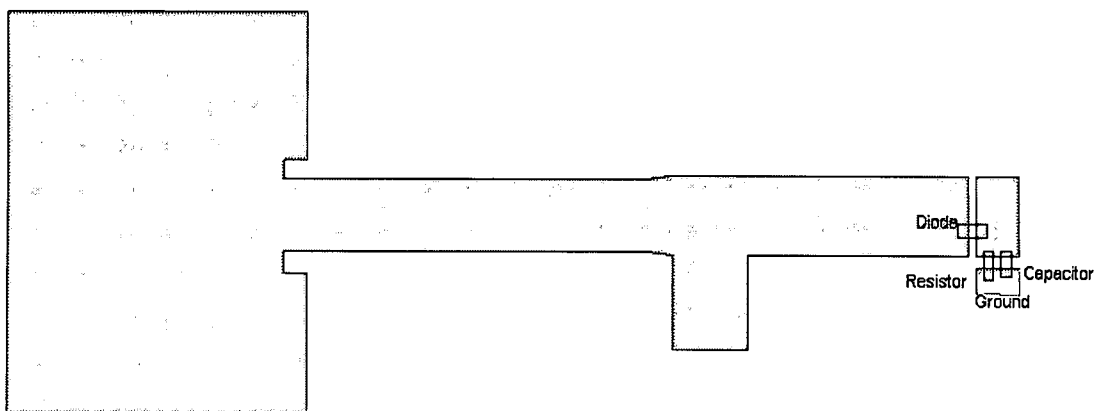


Fig.3.18 Top view of the rectifier antenna layout

In Figure 3.19, by supplying the input with the 15 MHz AC signal, the output is DC signal with the amplitude increasing with the input. When the input is low from 0 to 100 mV, the output is almost zero due the threshold voltage in the diode. For the Microwave testing, we need to illuminate the patch antenna with 2.45 GHz frequency power to test the output.

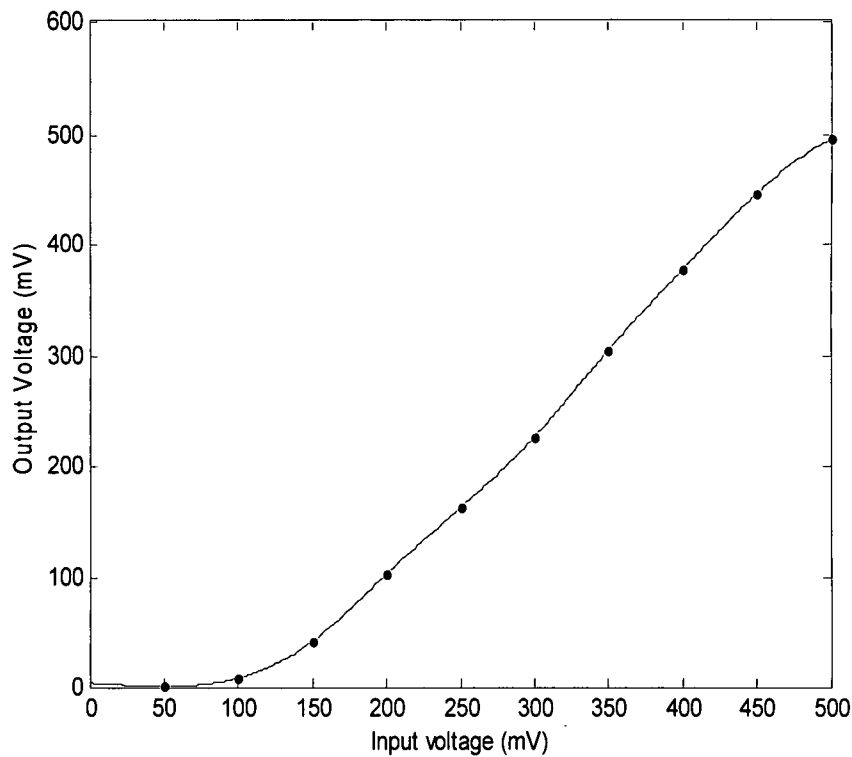


Fig.3.19 Measurement results at low frequency 15 MHz

CHAPTER 4

FREQUENCY TUNABLE ANTENNA DESIGN USING VARACTOR TECHNOLOGY

4.1 Motivation

In 2007, Emre Eridil et al. have reported a novel reconfigurable microstrip patch antenna that is monolithically integrated with RF micro-electromechanical systems (MEMS) capacitors for tuning the resonant frequency. Reconfigurability of the operating frequency of the microstrip patch antenna is achieved by loading it with a coplanar waveguide (CPW) stub on which variable MEMS capacitors are placed periodically. The sketch of the frequency tunable antenna is shown in Fig.4.1. MEMS capacitors are electrostatically actuated with a tuning voltage so that the antenna resonant frequency can continuously be shifted from 16.05 GHz down to 15.75 GHz as the actuation voltage is increased from 0 to 11.9V. It was the first monolithic frequency tunable microstrip patch antenna where a CPW stub loaded with MEMS capacitors is used as a variable load operating at low dc voltages at that time [29].

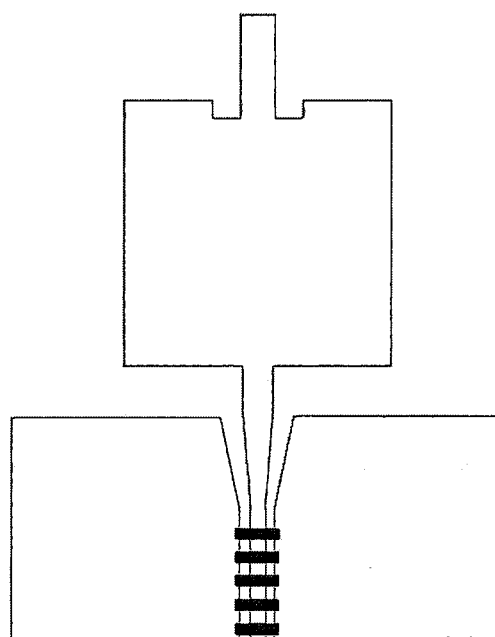


Fig.4.1 Schematic view of the frequency tunable microstrip patch antenna

However, compared with MEMS technology, ferroelectric varactor is better in terms of switching speed, integration capability etc. Guru Subramanyam in our group has developed a ferroelectric shunt switch based on varactor technology as shown in Fig. 4.2. Normally, the ferroelectric varactor enjoys advantages like low actuation voltage, high switching speed, good isolation, low packaging cost, low power consumption and very good integration capability compared with RF MEMS. Our motivation is to integrate the ferroelectric varactor with the patch antenna and achieve the function of tuning the resonant frequency.

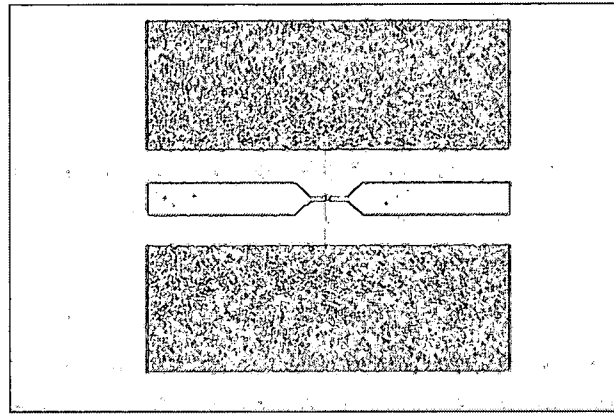


Fig.4.2 Top view of ferroelectric shunt switch based on varactor technology

4.2 Electrical equivalent model

The strategy of designing the tunable antenna with the aid of ferroelectric varactor is to make the antenna and varactor connect serially so that the electrical equivalent models of the antenna and ferroelectric varactor could be used. In the previous literature, the lumped element electrical equivalent model is of different types [57][58][59][60]. For simplicity, we adopt the three shunt RLC resonant circuit as the electrical equivalent model of the patch antenna shown in Fig.4.3. The values of resistance, inductance and capacitance can be chosen by investigating the S11 frequency response.

The electrical model for the ferroelectric varactor is shown in Fig.4.4. In this model, $C(V)$ is the test capacitance of the ferroelectric material, and $R(V)$ is the shunt resistance modeling leakage conductance of the capacitor. R_s and L are the parasitic series resistance and inductance of the capacitor respectively. When different voltages are applied, $C(V)$ will be changed accordingly so that the

tunable function can be achieved. By connecting the two components, the electrical model of the tunable antenna system is established.

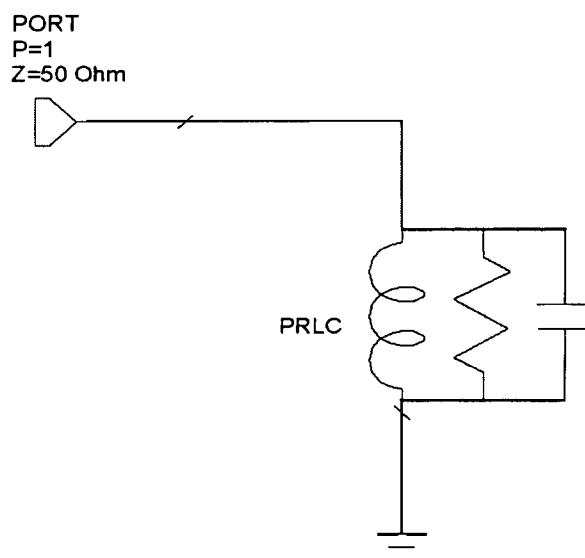


Fig.4.3 Equivalent electrical model for antenna

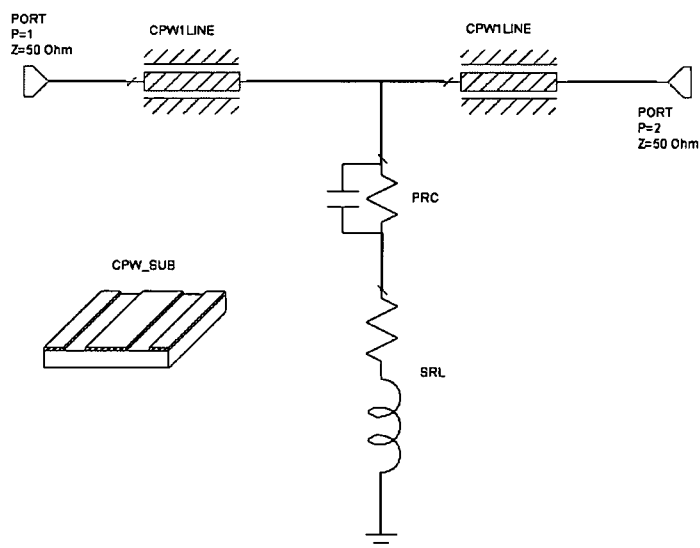


Fig.4.4 Equivalent electrical model for ferroelectric varactor

4.3 Electromagnetic layout

From the electrical model, it is not obvious to find the advantage of ferroelectric varactor integration. However, the electromagnetic layout gives a clear demonstration of the simplicity and convenience since there is no mechanical movement. For the MEMS capacitor, the tuning range of the antenna can be increased either by increasing the tuning range of the MEMS capacitors or by the use of variable capacitors at different places on both of the radiating edges to the antennas. These approaches are at the expense of an increase in the dc biasing and fabrication complexity. Figure 4.5 is an analogy of Figure 4.1 by replacing the MEMS capacitor with ferroelectric varactor. By applying different voltages on the signal line which is the middle conductor line, the resonant frequency is expected to change. The capacitance value can be altered also by changing the overlapping area of the capacitor.

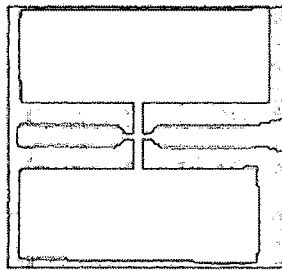


Fig.4.5 A sketch of tunable antenna integrated with ferroelectric varactor

4.4 Simulation results of electrical equivalent model

Based on the electrical equivalent model of antenna and shunt switch typed ferroelectric varactor, the electrical equivalent model of the frequency tunable antenna is proposed in the Figure.4.6. By changing the varactor capacitance from 0.21pF to 0.91pF, the resonant frequency of the antenna is changed accordingly.

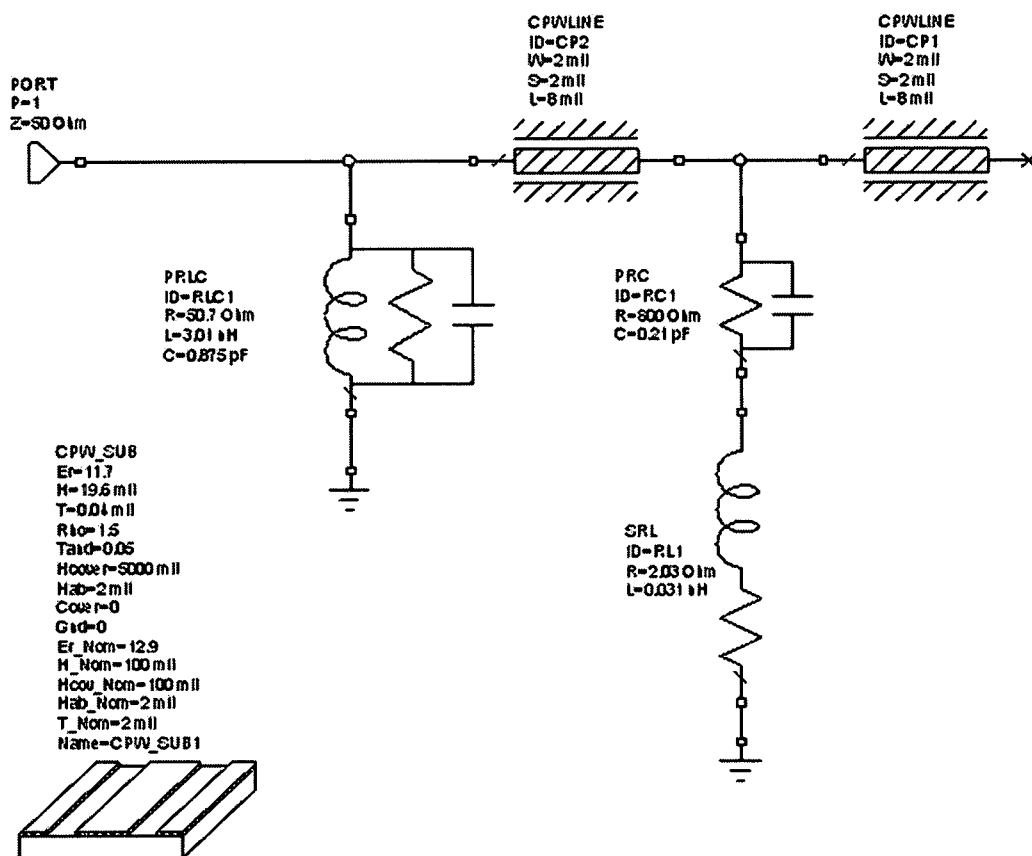


Fig.4.6 Equivalent electrical circuit of the tunable frequency antenna

In the Fig. 4.7, the simulation results of the S11 for the electrical equivalent circuit is shown with the frequency range of 1.5 – 3.5 GHz. The resonant frequency is

changing from 2.7 GHz to 2.2 GHz. The shift of frequency is 600 MHz. The tuning value of the capacitance is from 0.21pF to 0.91 pF which is based on the BST ferroelectric thin film.

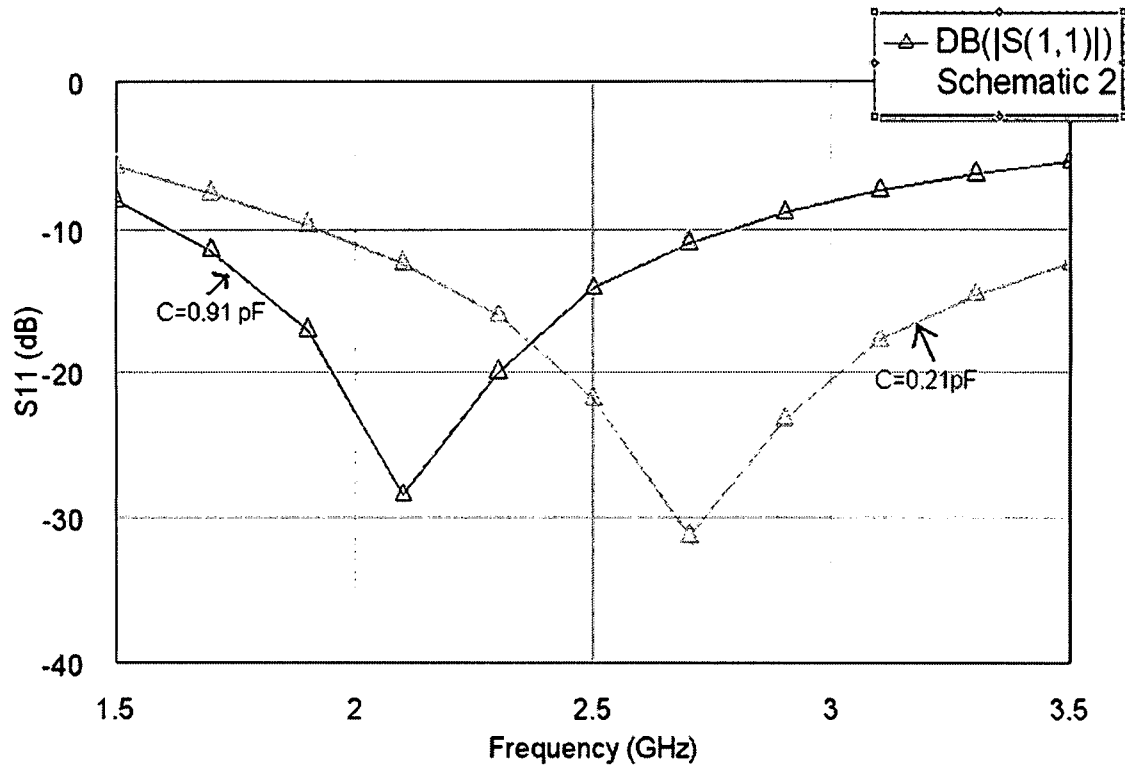


Fig.4.7 Simulation results of S_{11} for the electrical equivalent circuit of tunable frequency antenna

CHAPTER 5

EXPERIMENTAL RESULTS ON FERROELECTRIC THIN FILMS AND DEVICES

5.1 Electrical characterization for advanced electronic materials

Based on the electrical characterization techniques our capabilities were endowed with, measurements were done to disclose the electrical properties of advanced electronic materials including ferroelectric materials, biopolymers and etc.

5.1.1 Comparison of AC & DC resistance for PZT thin film capacitor

The electrical properties of PZT (Lead Zirconate Titanate) thin film are of great importance for its applications such as it is always expected to keep the current through the PZT as low as possible. Among those applications, PZT capacitors in the PCB circuits always have AC (alternating current) signal as its input while the drive profile of DRAM storage and non-volatile PZT memory normally is DC (direct current) signal. Especially with the trend of PZT capacitor used as an discrete component, such as EMC (electromagnetic compatibility) decoupling

capacitor [61], it is necessary to make investigations into the different influences of AC signal (Fig.5.1) and DC(Fig.5.2) on the electrical properties of PZT capacitor.

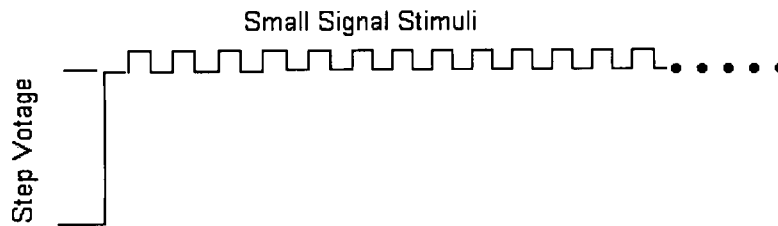


Fig.5.1 Drive profile of AC small signal measurement

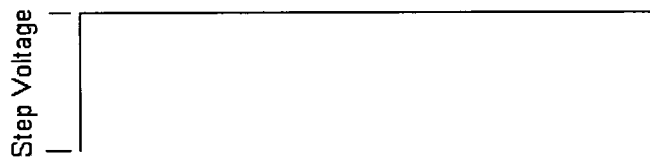


Fig.5.2 Drive profile of DC small signal measurement

The PZT capacitors used are a kind of commercial ones from Radiant Technology, Inc. The material used is 20/80 PZT. As a perovskite material ABO_3 , $Pb(ZrTi)O_3$ with lead in the A site and zirconium and titanium share the B site in a 20/80 population ratio. The capacitor measured is 2550 Å thick with an area of $1000 \mu m^2$. The maximum test voltage is 9 V. The electrode material is platinum. The structure of the PZT is shown in the Figure 5.3.

The AC resistance is measured by HP 4280A 1MHz C Meter/C-V Plotter. AC signal is at the frequency of 1 MHz with the signal level of 30 m Vrms, which is imposed on the step DC voltage. The value of resistance is the reciprocal of the

conductance, which is measured directly. The hold time (the period before the first measurement begins) is 5 s and the step delay (time period when the step voltage is applied) is 5 s. The measurement is shown in Figure 5.8.

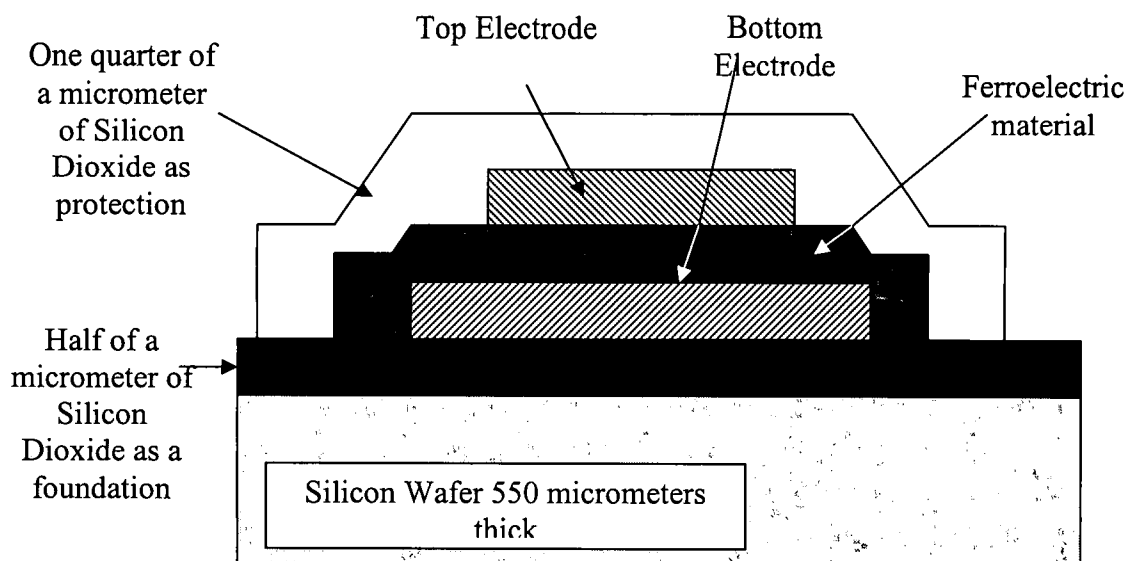


Fig.5.3 Cross section of a ferroelectric capacitor on a silicon wafer

(Courtesy of Radiant Technology)

The DC resistance is measured by Precision LC Tester from Radiant Technology in Figure 5.6. The resistance values are derived from leakage current measurements (I-V curve). The difference between AC and DC measurement is that there is no small alternating signal stimuli applied on the step voltage. The detailed drive profile in the Vision software is in Figure 5.4. The soak time is set to be 1000 ms. Measurement time is 1ms and the step delay is 1000 ms. The initial bias voltage was 9 V and the delay time was 1 ms. The DC resistance is

related to leakage current, which depends on fabrication condition and measurement procedures [62].

The trend of AC resistance increasing with voltage can be explained by the effect of tunable capacitance. Such an inverted" butterfly loop" is typical of a ferroelectric material of small signal measurement. When the applied voltage is increased, the capacitance reaches its maximum value at the voltage of 2V and decreases as shown in Figure 5.5. So it is observed that AC resistance reached its minimum at the voltage of 2V and then increases as the voltage increases. R_p , the leakage resistance of the thin film, is not constant but a function of frequency. With the increase of frequency, the loss tangent will increase so the resistance will decrease accordingly.

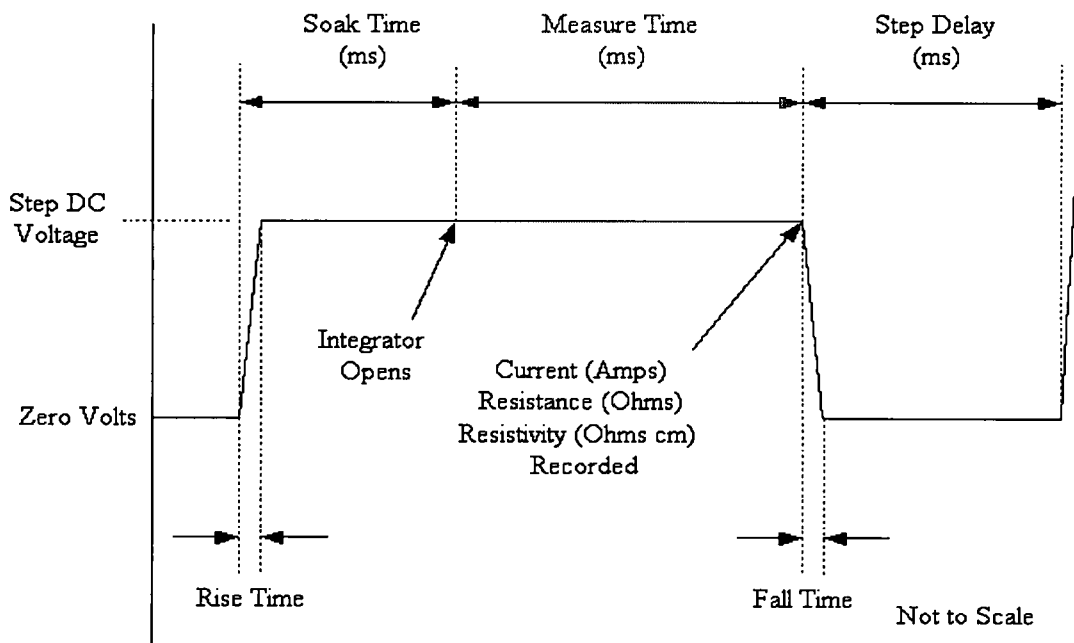


Fig.5.4 Drive profile for resistance measurement by radiant tester

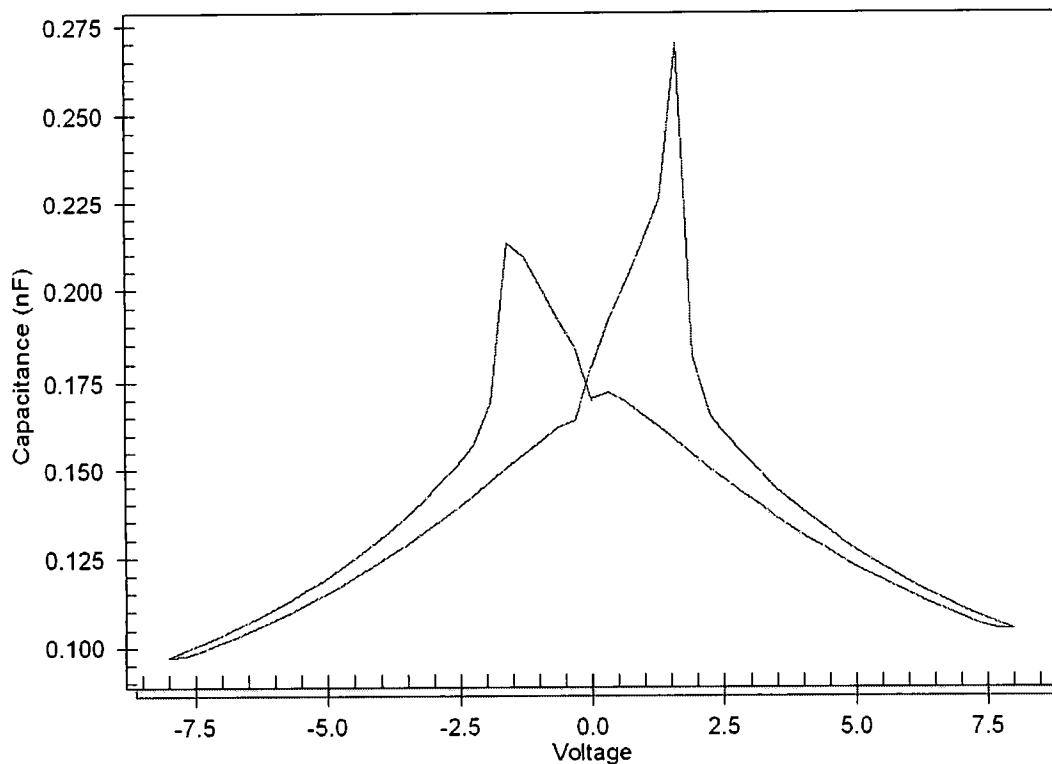


Fig.5.5 C-V curve of the PZT thin film capacitor

A commonly used equivalent circuit for a capacitor is used to investigate the problem [63] in Figure 5.7, where

R_s : Series resistance from leads

L_s : Series inductance from leads

R_p : Leakage resistance of the thin film

C_p : Capacitance of the thin film

The impedance of the equivalent circuit is

$$Z = R_s + j\omega L_s + \frac{R_p \frac{1}{j\omega C_p}}{R_p + \frac{1}{j\omega C_p}} = (R_s + \frac{R_p}{1 + \omega^2 C_p^2 R_p^2}) + j\omega(L_s - \frac{C_p R_p^2}{1 + \omega^2 C_p^2 R_p^2})$$

Based on the electrical model, the measured resistance is the real part of the impedance (R). Considering both DC and AC resistance measurements, R_s is approximately 10^5 Ohm and R_p is around 10^{10} Ohm at the frequency of 1MHz. From the C-V curve (Capacitance versus Voltage), C_p is the tunable capacitance of the value between 5pF and 35pF.

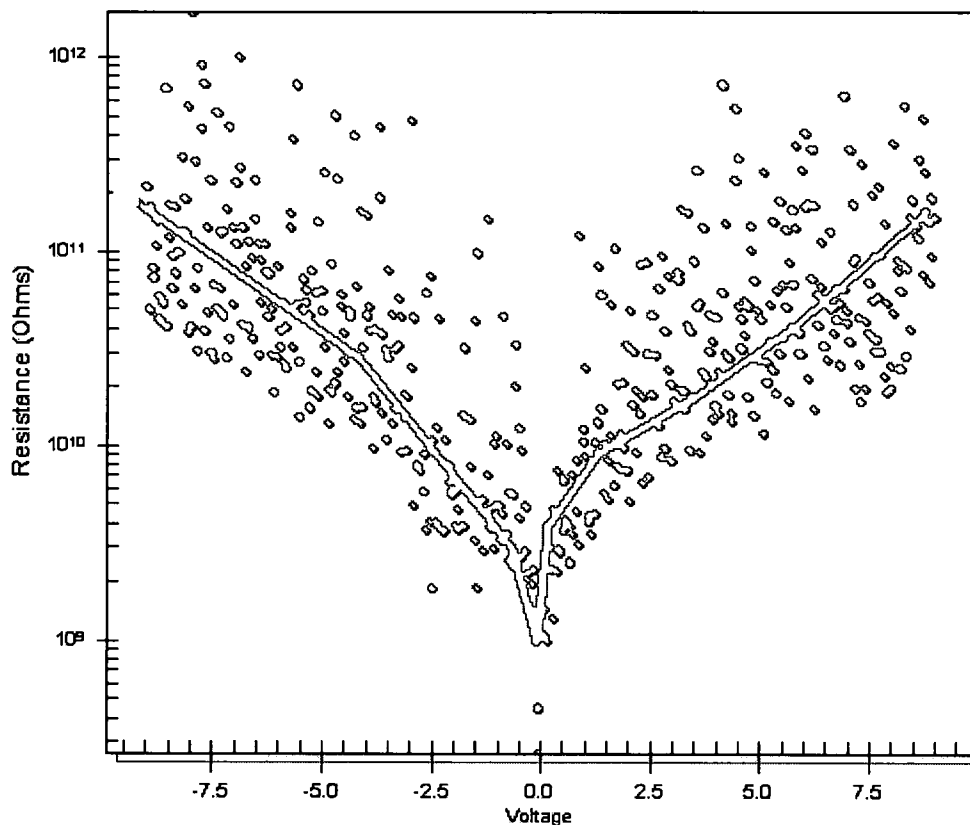


Fig.5.6 DC resistance of the PZT thin film capacitor

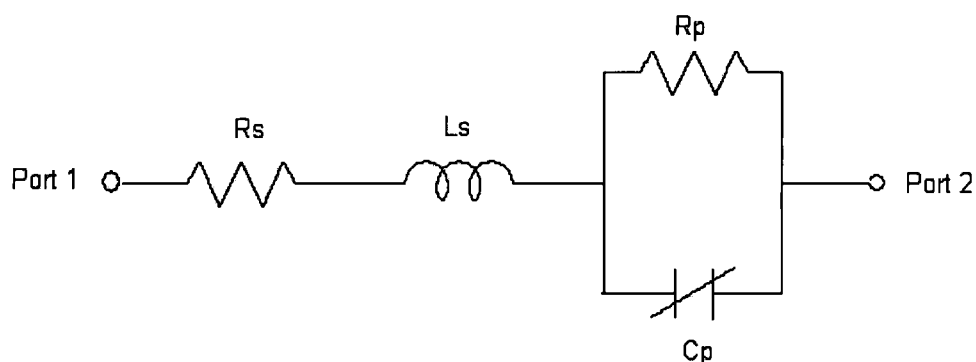


Fig.5.7 An equivalent circuit for ferroelectric thin film capacitor

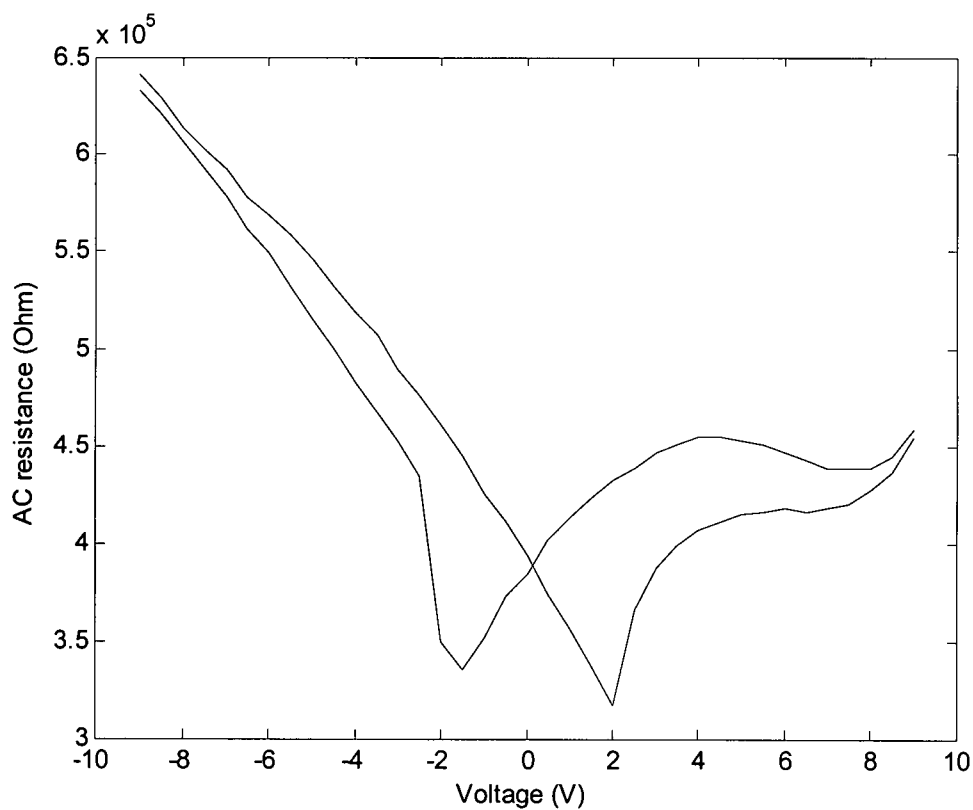


Fig.5.8 AC resistance of the PZT thin film capacitor

The result that DC resistance is different from the AC resistance can be explained by the electrical model as well as a physical mechanism. AC

resistance is much smaller than the DC resistance because the alternating signal will promote electron de-trapping process so that the apparent resistance will be less than that of DC signal profile [64][65]. Such a difference points out that the various drive signals have different impacts of electrical properties of the capacitors. While resistance is not a direct quantity to describe the conduction mechanism like current, it still tends to behold the origin of trap related bulk controlled mechanism in the PZT capacitor. Phenomenon of AC resistance resonance is due to the tunability of PZT capacitance which contributes to the minimum value of AC resistance.

5.1.2 Hysteresis loop of the BT2 peptide-induced BaTiO₃

By collaborating with Georgia Tech University, the feasibility of peptides identified by phage display capable of inducing the rapid, room-temperature formation of tetragonal barium metatitanate, BaTiO₃, from an aqueous precursor solution at near neutral pH. Traditionally, many chemical methods were employed to synthesize BaTiO₃ (like mixed salt, sol-gel, vapor-diffusion sol-gel, microemulsion, co-precipitation, polymeric precursor, etc). However, the formation of ferroelectric (tetragonal) BaTiO₃ by such approaches has required heat treatment at $\geq 500^{\circ}\text{C}$ for $\geq 1\text{h}$. For example, tetragonal BaTiO₃ has been produced via hydrothermal synthesis at 240°C , but only after prolonged annealing ($\geq 9\text{h}$) under highly alkaline conditions.

A new method of rapid bioenabled formation of ferroelectric BaTiO₃ at room temperature from an aqueous salt solution at near neutral pH was developed by using a synthetic peptide-like bolaamphiphile, bis(N- α -amidoglycylglycine)-1, 7-heptane dicarboxylate, which can induce the room-temperature precipitation of ferroelectric BaTiO₃ [66].

The electric field-induced polarization of the BaTiO₃ was evaluated with a Radiant Technologies' Precision LC tester. As shown in Figure 5.10, the BaTiO₃ particle layer exhibited polarization hysteresis, which is a well-known characteristic of ferroelectric materials. The slope of the P-E curve at low field yielded a relative permittivity value of ~ 2200 , which is comparable to values reported for BaTiO₃ of 100-300 nm crystal size[67][68]. The leakage current was measured below 10^{-7} A up to a bias voltage of ± 10 V, which is low and showing promise for its low power applications [69].

The present work demonstrates, for the first time, that a phage display isolated peptide can induce the room-temperature formation of ferroelectric (tetragonal) BaTiO₃ within 2 hours from an aqueous precursor solution at near neutral pH. The ability of peptides to promote the rapid formation of functional crystalline multi-component ceramics under ambient conditions provides new opportunities for the integration of such functional materials with low-temperature or reactive materials and substrates (e.g., with polymers, bio-organics, or silicon).

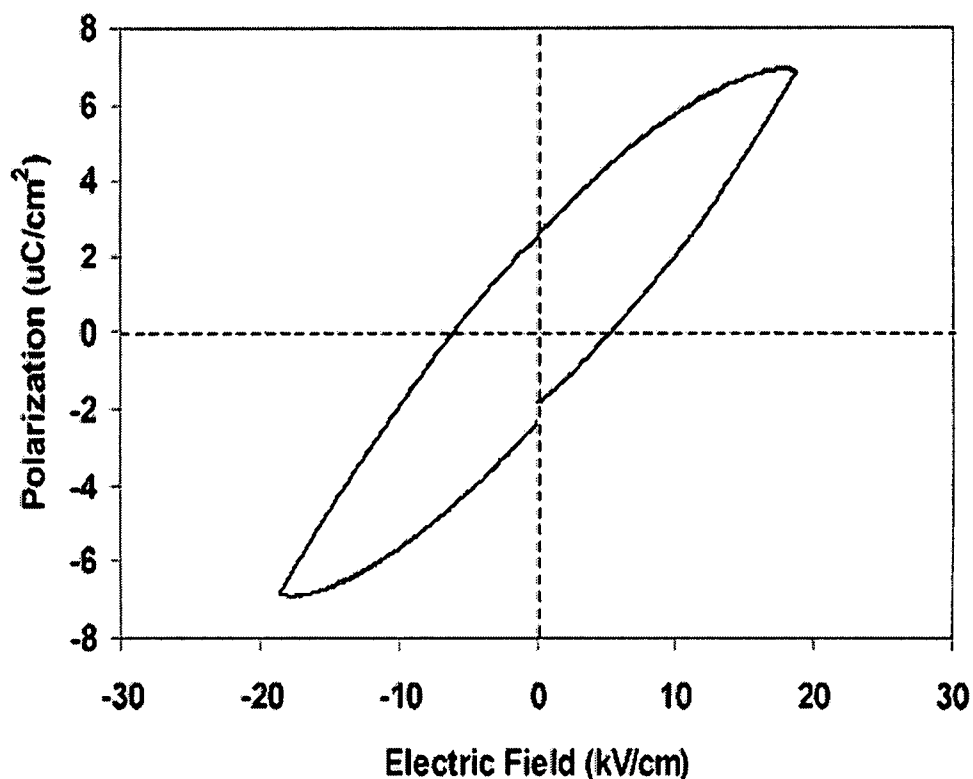


Fig.5.9 Polarization versus applied electric field at 1 kHz for the peptide-induced BaTiO_3

5.1.3 Leakage current measurement for fiber nanotube junction

There has been a lot of research on nanotubes recently [70]. Based on our electrical properties characterization systems, the I-V curve was measured to study the conduction mechanism of fiber nanotubes, which is placed between the two junctions. The measurement is shown in Figure.5.10. As the voltage is increasing, the current is enhancing accordingly. At the 0.5V, the current is increasingly jumping, which may be due to the Pool-Frenkel conduction associated with field enhanced thermal excitation of charge carriers from internal

traps [71]. The pool-Frenkel current density is give by: [72]

$$J_{PF} \sim E \exp\left[-\frac{q}{kT\left(\varphi - \sqrt{\frac{qE}{\pi \epsilon_0}}\right)}\right] , \quad \text{where } \varphi \text{ is the barrier height.}$$

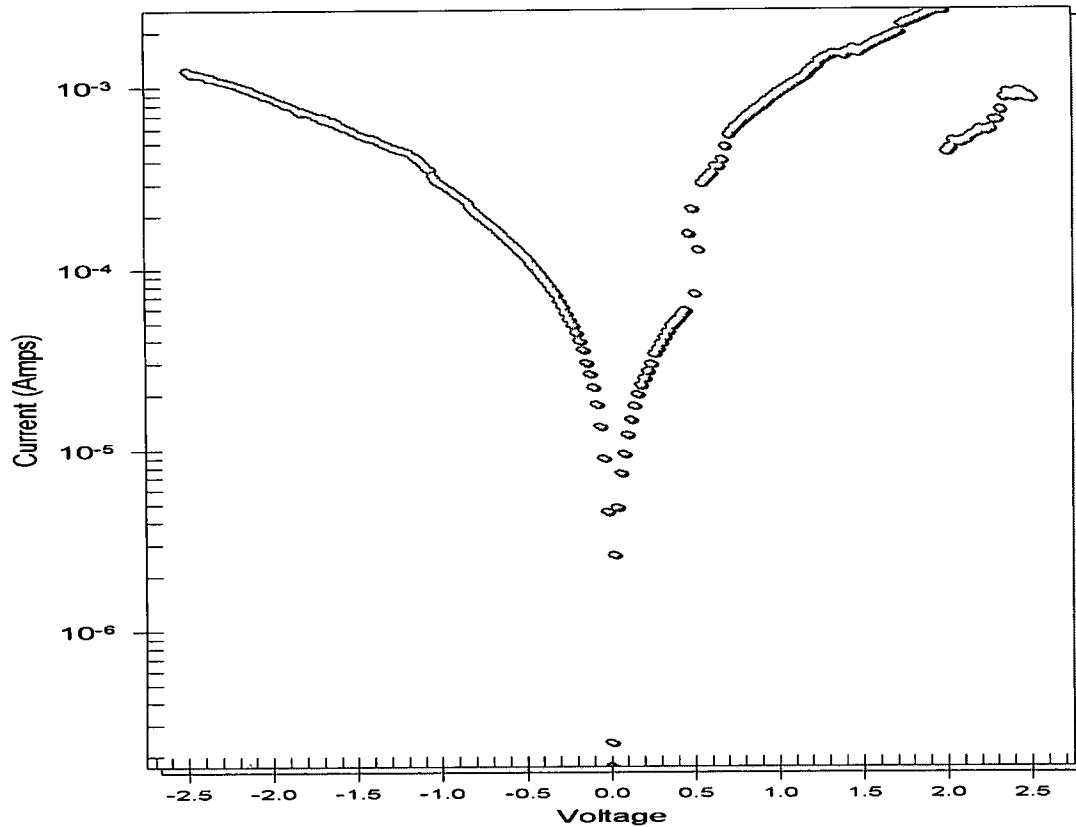


Fig.5.10 I-V curve of fiber nanotube junction

5.2 RF performance of varactor shunt switch

5.2.1 Frequency dependent impedance relationship of varactor shunt switch

To integrate the varactor shunt switch into the microwave circuit, we need to investigate the impedance of varactor shunt switch. The normalized input impedance at the input port can be obtained from S11 as:

$$S_{imp} = \frac{1 + S_{11}}{1 - S_{11}}$$

Figure 5.11 describes how S_{11} and S_{21} are tuned with different applied voltages. With the applied voltage increasing, S_{21} is increasing so that the switch can be thought as “on” state.

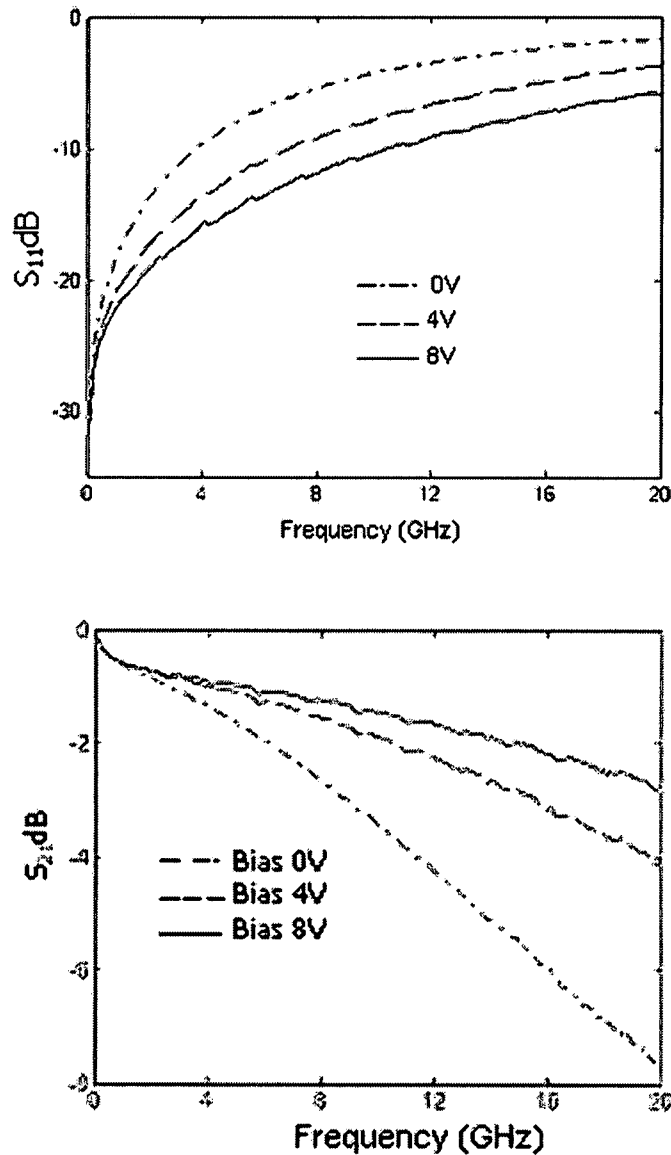
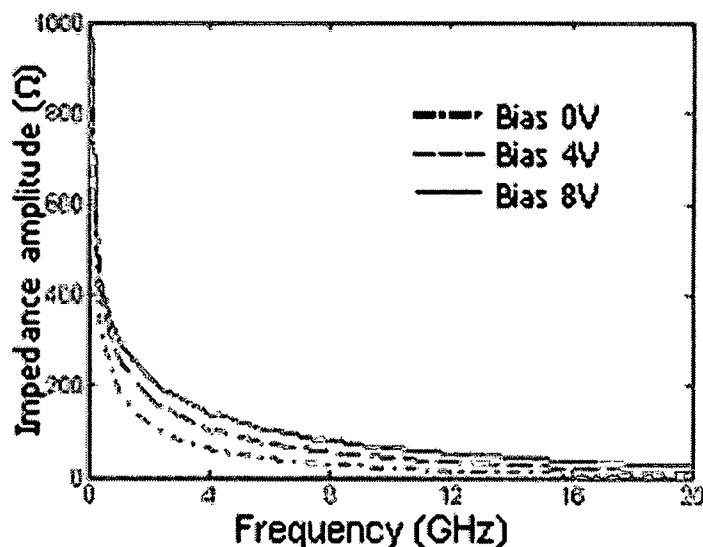
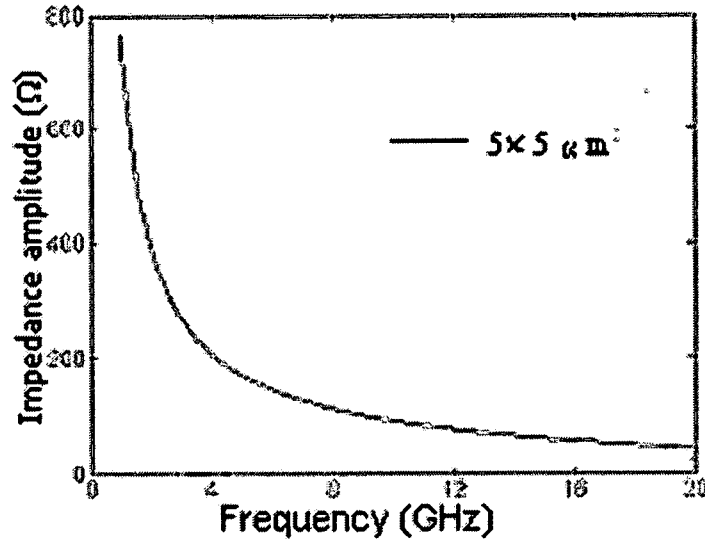


Fig 5.11 Microwave measurements of the $5 \times 5 \mu\text{m}^2$ device

Fig.5.12 gives the comparison of extracted capacitor impedance and simulated impedance for the $5 \times 5 \mu\text{m}^2$ device. A typical impedance property of a capacitor is described in [61]. The impedance can be considered as a series combination of a capacitance, inductance and a resistance. At low frequency, the impedance reduces with frequency since the capacitance dominates the impedance. At a frequency when the inductance and capacitance resonates, the impedance reaches its minimum which is equal to the resistance. After that the impedance increases with frequency since the inductance dominates. For capacitor with an area of $5 \times 5 \mu\text{m}^2$, the impedance reduces with the sweeping frequency in all the measured frequency range. No resonance takes place. In [61], the significant series resistance is attributed to the interface. Hence, no obvious interface resistance was found.



(a) Extracted capacitor impedance



(b) Simulated Impedance

Fig 5.12 Comparison of extracted capacitor impedance and simulated impedance for $5 \times 5 \mu\text{m}^2$ device

5.2.2 Temperature dependent performance of varactor shunt switch

Based on the previous studies, temperature has influence on the dielectric properties of BST material [73][74][75]. It is necessary to investigate the relationship between scattering parameters and temperatures. The electric thermal controller is used to vary the temperature by heating the chuck. The temperature range is from 10°C to 100°C . The measurement result is shown in the following figures. The variation of S_{11} is not much as reported in Figure 5.13. However, the temperature has much influence on S_{21} as shown in Figure 5.14. The higher the temperature, the larger the S_{21} value since the dielectric constant is decreasing with temperature.

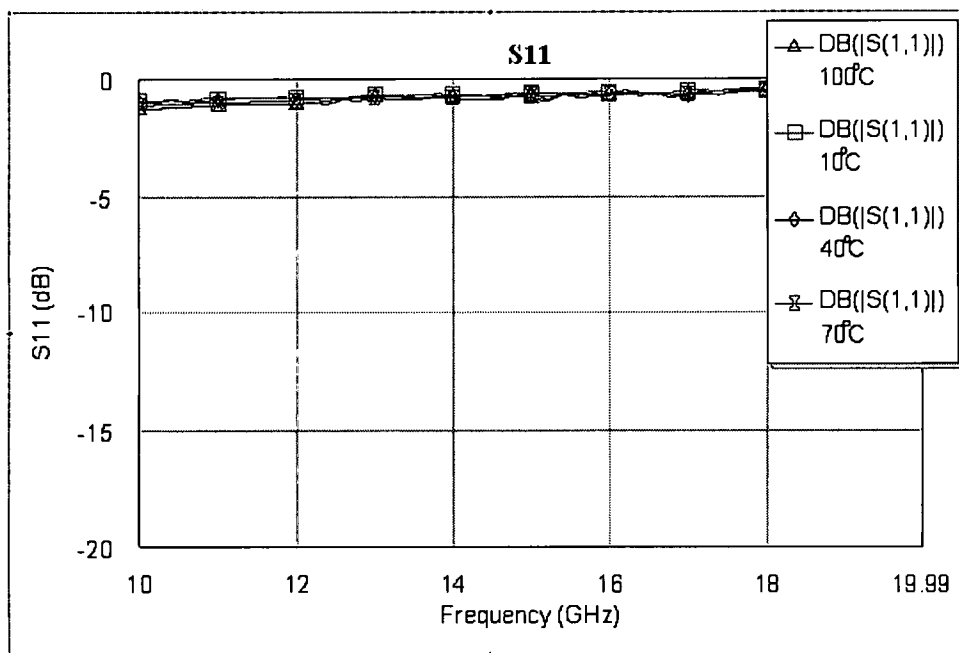


Fig 5.13 Temperature dependence of S_{11} for varactor on Sapphire at 0V

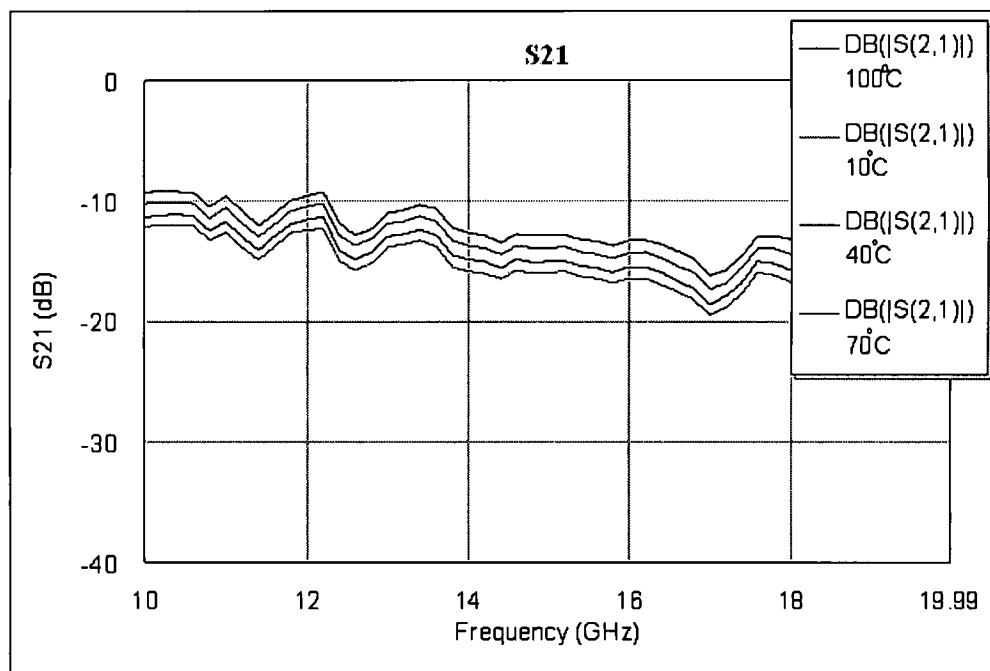


Fig 5.14 Temperature dependence of S_{21} for varactor on Sapphire at 0V

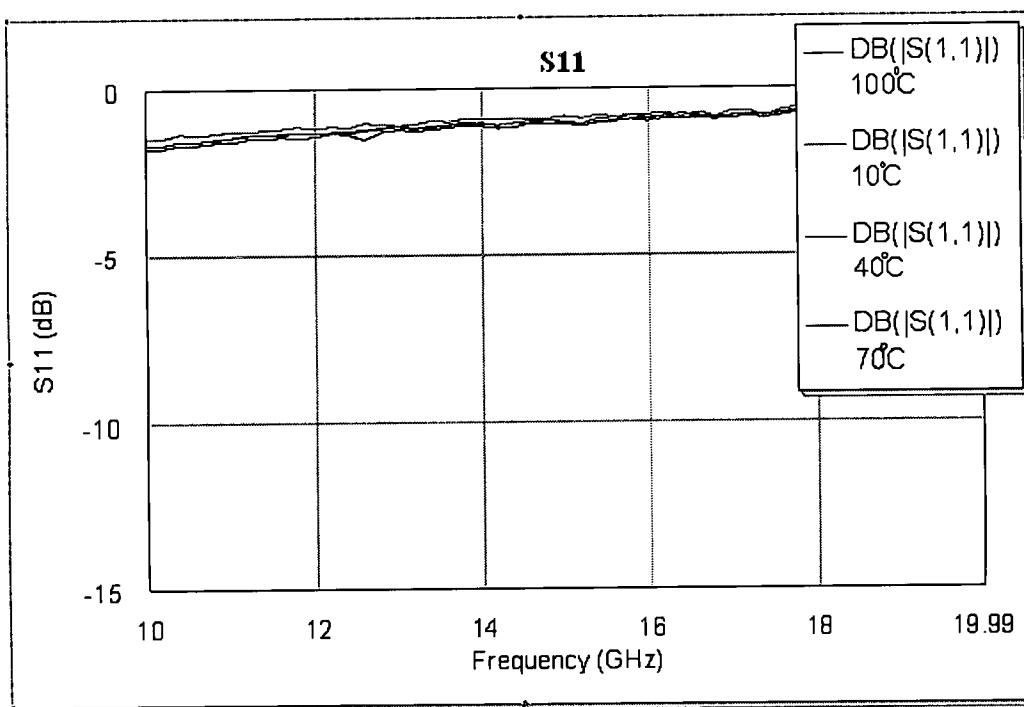


Fig 5.15 Temperature dependence of S11 for varactor on Sapphire at 2V

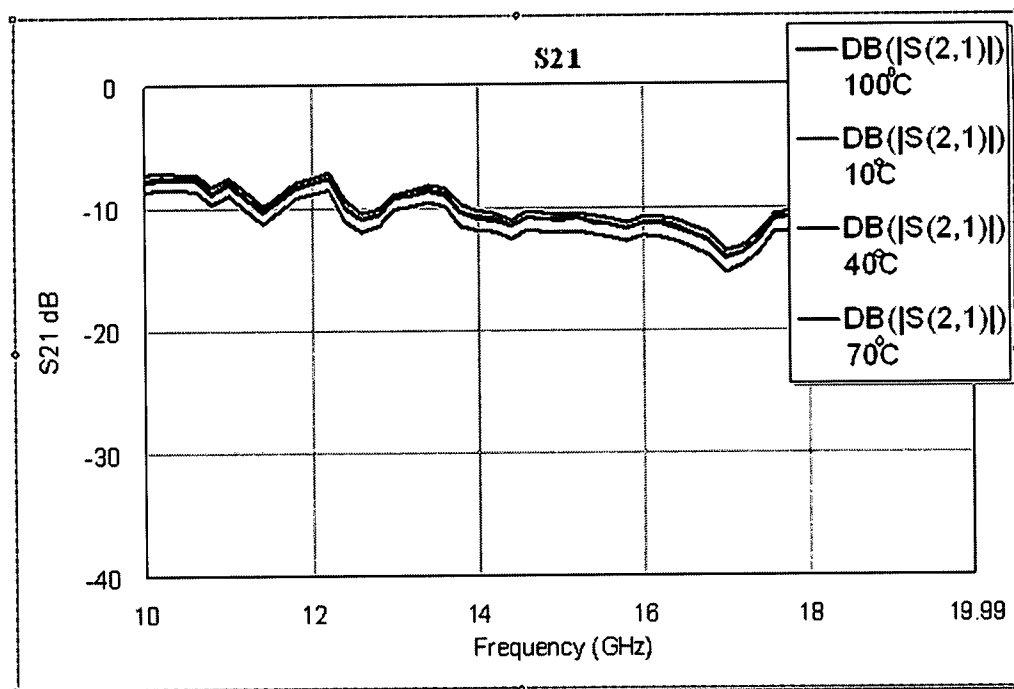


Fig 5.16 Temperature dependence of S21 for varactor on Sapphire at 2V

In the Figure 5.15 and Figure 5.16 above, measurements were conducted when 2 volt is applied. Compared with the situation when no applied is applied, the S11 is still not changed much when voltage is applied. However, the S21 does not change much at higher temperature but changes significantly at 10°C, by about 10%.

5.2.3 Dielectric property of BST thin film based on Varactor Shunt Switch

Based on the capacitive test structure of varactor shunt switch, the dielectric property of BST thin film can be obtained by matching the experimental scattering parameters data to the electrical modeled results.

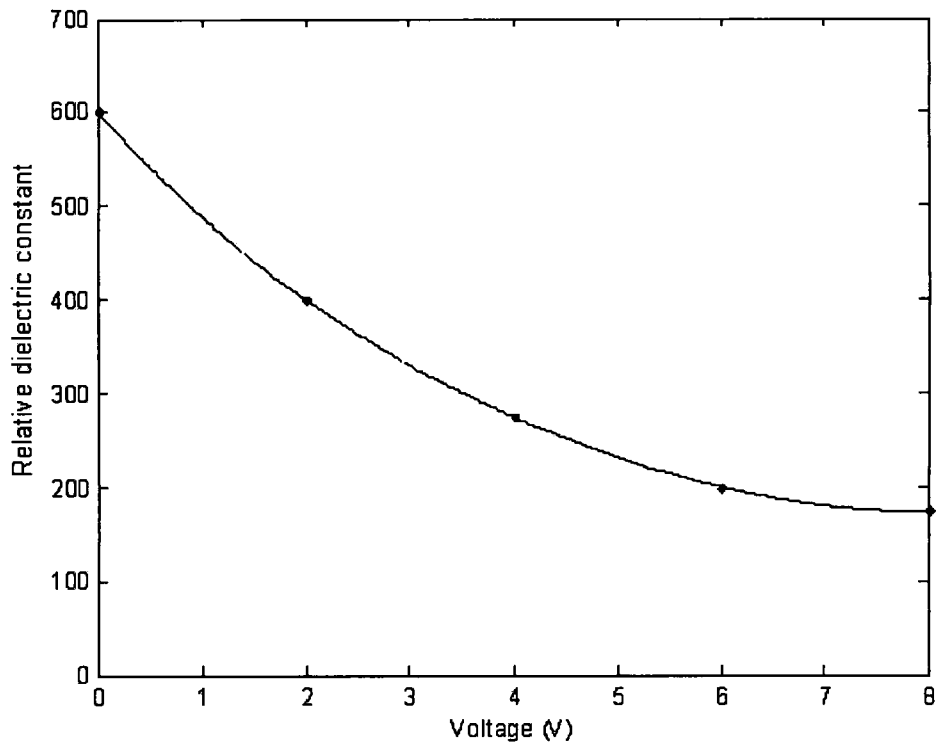


Fig 5.17 Voltage dependent dielectric constant of Ba_{0.6}Sr_{0.4}TiO₃

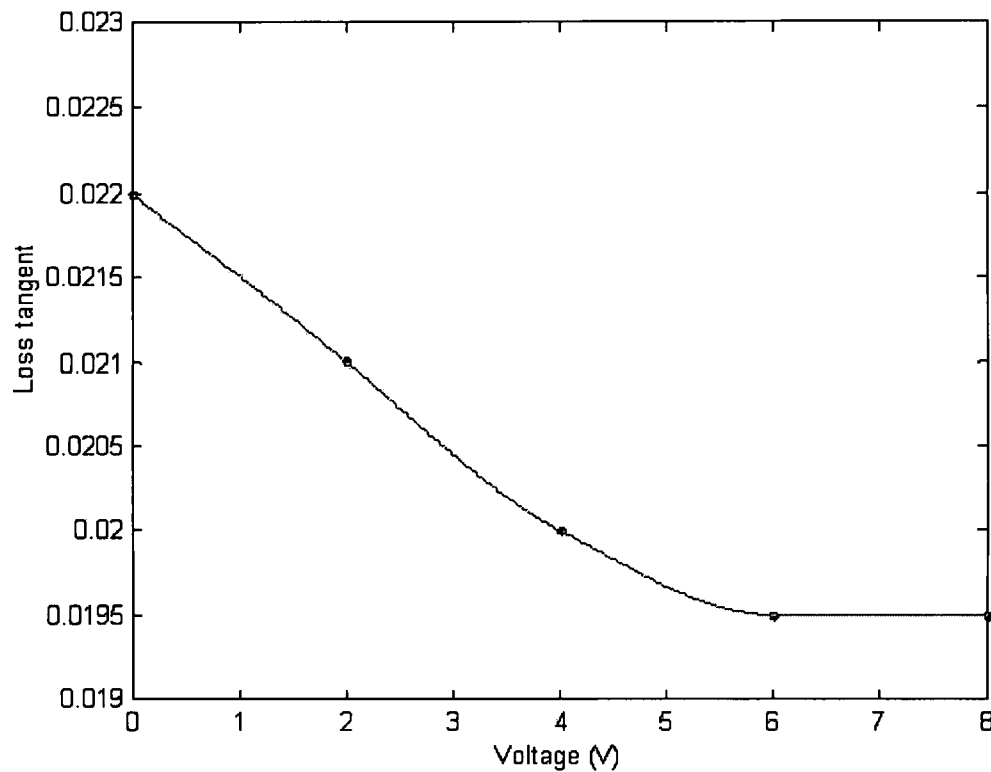


Fig 5.18 Voltage dependent loss tangent of $\text{Ba}_{0.6}\text{Sr}_{0.4}\text{TiO}_3$

In Figure 5.17 and 5.18 above, the dielectric properties are shown. The dielectric constant is decreasing with the applied voltage, which presents a nonlinear relationship. Loss tangent is declining with the applied voltage while the value remains constant at the upper voltage end. As shown in Figure 5.19, the relationship between temperature and dielectric constant can be derived by matching electrical model and experimental data. The dielectric constant decreases with the temperature. While the relationship between dielectric constant and temperature is dependent on thickness and frequency, Figure 5.19 is presented reasonably when the thickness of $\text{Ba}_{0.6}\text{Sr}_{0.4}\text{TiO}_3$ is $0.4\mu\text{m}$ with the frequency range between 10 GHz and 20 GHz [76]. Figure 5.20 describes the

temperature dependent dielectric loss relationship, which indicates a very low loss for $\text{Ba}_{0.6}\text{Sr}_{0.4}\text{TiO}_3$ fabricated on sapphire substrate.

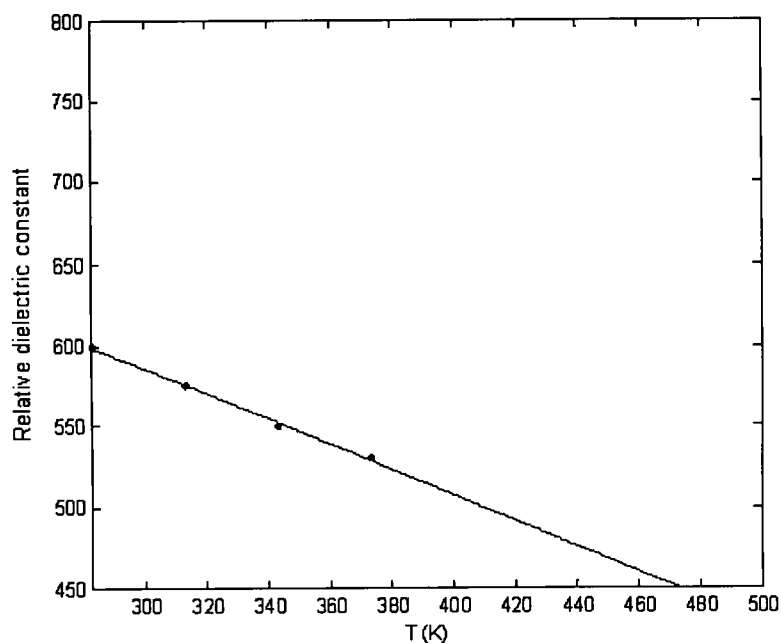


Fig 5.19 Temperature dependent dielectric constant of $\text{Ba}_{0.6}\text{Sr}_{0.4}\text{TiO}_3$ at 0V

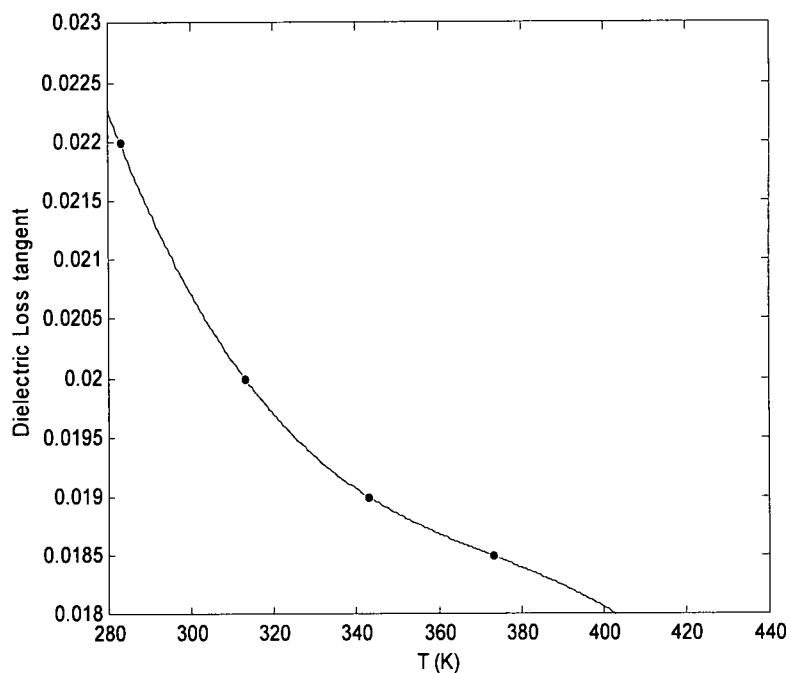


Fig 5.20 Temperature dependent dielectric loss of $\text{Ba}_{0.6}\text{Sr}_{0.4}\text{TiO}_3$ at 0V

CHAPTER 6

SUMMARY AND FUTURE WORK

6.1 Summary

This thesis consists of two major parts: electrical property characterization techniques and RF antenna rectifier design. Characterizations of the novel electronic materials are divided into two categories: low frequency and microwave frequency measurements. By using different drive profile as the input signal, we found the differences between AC & DC resistance of PZT ferroelectric capacitors. Microwave characterization of the ferroelectric capacitors was done using the varactor shunt switch structure, and measuring the scattering parameters. The feasibility of a rapid bio-enabled approach to form ferroelectric BaTiO₃ at room temperature from an aqueous salt solution at near neutral pH was demonstrated by collaborating with Georgia Tech. Also research on the frequency tunable frequency integrated with shunt switch ferroelectric varactor has been initiated and simulation results are presented.

6.2 Future work

The antenna rectifier will be tested in the microwave frequency range. Also the tunable frequency antenna should be investigated further to make it function as well. The conduction mechanism should be fully understood when measuring different electronic materials by Radiant Tester. The optimization of the antenna rectifier can be performed to increase the output voltage and decrease the input threshold RF power that is the minimum value required to produce the DC voltage.

BIBLIOGRAPHY

- [1] C.B. Sawyer, C.H. Tower, "Rochelle salt as a dielectric", Physical Review, Vol.35, 1930, pp 269- 273
- [2] G.H. Haertling. "Ferroelectric Ceramics: History and Technology", Journal of the American Ceramic Society, Vol.82 4, 1999, pp 797-818
- [3] D. Damjanovic, "Ferroelectric, dielectric and piezoelectric properties of ferroelectric thin film and ceramics", Reports on Progress in Physics 61 (9), 1998, pp 1267-1324
- [4] G.H. Haertling, "Ferroelectric thin films for electronic applications", Journal of Vacuum Science and Technology, 9 (3), 1991, pp 414-420
- [5] JM.Liu, WM. Wang, ZG. Liu, HL. Chan, CL.Choy, "Dynamic hysteresis in ferroelectric systems: experiment and Monte Carlo simulation", Applied Physics A-Materials Science & Processing, Vol:75, 2002, pp 507-514
- [6] C.J.Dias, D.K.Das-Gupta, "Hysteresis measurements on ferroelectric composites", Journal of Applied Physics, Vol:74, 1993, pp 8317-8321
- [7] FD.Flaviis, N.G.Aloxopoulos. "Planar microwave integrated phase- shifter design with high purity ferroelectric material", IEEE Transaction on Microwave Theory and Techniques, VOL 45, No 6, 1997,pp 963-969
- [8] G.Rupprecht and PO.Bell "Microwave losses in strontium titanate above the phase transition", Physical Review, 20, 1915, pp 123

- [9] M J Lancaster, J Powell and A Porch. "Thin-film ferroelectric microwave devices", Superconductor Science and Technology, 11, 1998, pp 1323-1334
- [10] A.K.Tagantsev, V.O.Sherman, K.F.Astafiev, J.Venkatesh & N.Setter. "Ferroelectric Materials for Microwave Tunable Applications", Journal of Electroceramics, 11, 2003, pp 5-66
- [11] YH.Chun, JS.Hong , "BST-Varactor Tunable Dual-Mode Filter Using Variable Z_C Transmission Line", IEEE Microwave and Wireless Components Letters, Vol.18, 2008, pp 167-169
- [12] G. Subramanyam, K. Pasala , "Ferroelectric varactor shunt switches for broadband phase control applications", Integrated Ferroelectrics, Vol 93, 2007, pp 101-109
- [13] CL. Fu, FS. Pan, HW. Chen, "International journal of infrared and millimeter waves", Vol 28, 2007, pp 229-235
- [14] L. Vincent, A. Rousseau, "Ferroelectric-based agile devices-application to tunable filters", International Journal of RF and Microwave Computer-Aided Engineering, Vol 17, 2007, pp 56-62
- [15] OY. Buslov, VN. Keis, IV. Kotelnikov, "Slot-line ferroelectric phase-shifters and phase-array antenna on their base", Integrated Ferroelectrics, Vol 86, 2006, pp 125-130
- [16] OY. Buslov, CY. Kang, "Dielectric resonators loaded by ferroelectric varactors for tunable Ka band filter", Integrated Ferroelectrics, Vol 86, 2006, pp 171-179

- [17] G. Subramanyam, F. Ahamed, R. Biggers, A. Campbell, R. Neidhard, E. Nykiel, R. Cortez, K. Stamper, M. Calcaterra, "A new ferroelectric varactor shunt switch for microwave and millimeter-wave reconfigurable circuits", *Frequenz*. Vol 59, 2005, pp 37-40
- [18] JY. Kim, AM. Grishin, "Niobate-tantalate thin films microwave varactors", *Thin Solid Films*, Vol 515, 2006, pp 619-622
- [19] A. Jamil, TS. Kalkur, N. Cramer, "Voltage-controller oscillator design using ferroelectric varactors", *Integrated Ferroelectrics*, Vol 81, 2006, pp 157-163
- [20] P.J. Rainville and F.J. Harackewiez, "Magnetic tuning of a microstrip patch antenna fabricated on a ferrite film", *IEEE Microwave Guided Wave Letters*, 2, 1992, pp 483-485.
- [21] D.M. Pozer, "Radiation and scattering characteristics of microstrip antennas on normally biased ferrite substrate", *IEEE Trans Antennas Propagation* 40, 1992, pp 1084-1092
- [22] P.K. Misra, S.S. Pattnaik, and N. Das, "Tuning of microstrip antenna on ferrite substrate, *IEEE Trans Antennas Propagation*", Vol 41, 1993, pp 230-233
- [23] S.N. Das and S.K. Chowdhury, "Rectangular microstrip antennas on ferrite substrates", *IEEE Trans Antennas Propagation*", AP-30, 1982, pp 499-502
- [24] K.A. Jose, V.K. Varadan, V.V. Varadan. "Experimental investigations on electronically tunable microstrip antennas", *Microwave and Optical Technology Letters*, Vol 20, Issue 3, pp 166-169
- [25] PT. Teo, KJ. Vinoy, KA. Jose, VK. Varadan, W. Varadan, YB. Gan, "Design and development of tunable multi-layer smart antennas using ferroelectric

materials", Journal of Intelligent Material Systems and Structures, Vol 11, pp 294-299

[26] R.N.Simons, D.Chun, and L.P.B.Katehi, "Microelectromechanical systems (MEMS) actuators for antennas reconfigurability," IEEE MTT-S Int. Microwave Symp, Digest, 2001, pp.215-218

[27] R.N.Simons, D.Chun, L.P.B.Katehi, "Polarization reconfigurable patch antenna using Microelectromechanical Systems (MEMS) actuators," IEEE AP-S Symp. Digest, 2002, pp.6-9

[28] J.C.Chiao, S.-Y.Cheng, J.L.Chang, I.M.Chio, Y.Kang, and J.Hayasaka, "MEMS reconfigurable antennas," Int. J.RF Microwave CAE, Vol. 11, 2001, pp. 301-309

[29] E.Erdil, K.Topalli, M.Unlu, O. A.Civi, and T.Akin, "Frequency Tunable Microstrip Patch Antenna Using RF MEMS Technology", IEEE Transactions on Antennas and Propagation, VOL.55, No.4, 2007, pp 1193-1196

[30] J.Evans, "Understanding Ferroelectric Materials Test Tutorial" .Radiant Technology, 2006, <http://www.ferrodevices.com/>

[31] M.Dawber, I.Farnan and J.F.Scott, "A classroom experiment to demonstrate ferroelectric hysteresis". American Journal of Physics. 71 (8), 2003, pp 819-822

[32] D.Galt, JG.Price, "Characterization of a tunable thin film microwave $\text{YBa}_2\text{Cu}_3\text{O}_{7-x}/\text{SrTiO}_3$ coplanar capacitor", Applied Physics Letter, 63 (22), 1993, pp3078-3080

- [33] D.Galt, JG.Price, "Ferroelectric Thin Film Characterization Using Superconducting Microstrip Resonators", IEEE Transaction on Applied Superconductivity, VOL. 5, No. 2, 1995, pp 2575-2578
- [34] Q. Meng, X. Zhang, F. Li, J.Huang, X. Zhu, D. Zheng, B. Cheng, Q. Luo, C. Gu, Y. He, "Ferroelectric thin-film characterization using a coplanar waveguide bandstop filter", Physical status solidi, Vol 203, 2006, pp 379-385
- [35] M.Ouaddari, S.Delprat, F.Vidal, M. Chaker, and K. Wu, "Microwave Characterization of Ferroelectric Thin-Film Materials", IEEE Transactions on Microwave Theory and Techniques, Vol 53, No.4, 2005, pp1390-1397
- [36] G.Subramanyam, F.Ahamed, R.Biggers, "RF performance evaluation of ferroelectric varactor shunt switches", Microwave and Optical Technology Letters, Vol: 47, Issue: 4, 2005, pp 370-374
- [37] G.Subramanyam, F.Ahamed, R.Biggers "A Si MMIC compatible ferroelectric varactor shunt switch for microwave applications", IEEE Microwave and Wireless Components Letters, Vol: 15, Issue: 11, 2005, pp 739-741
- [38] G.Subramanyam, "A new method for electrical characterization of ferroelectric thin films at microwave frequencies", Ferroelectrics, Vol: 356 2007, pp 445-448
- [39] CM.Bartsch, G. Subramanyam, J. Grote, FK Hopkins, LL Brott, RR Naik, "A new capacitive test structure for microwave characterization of biopolymers", Microwave and Optical Technology Letters. Vol 49, Issue 6, 2007, pp 1261-1265
- [40] M. Cheney, Tesla, Man out of Time. Englewood Cliffs, NJ: Prentice Hall, 1981

- [41] W. C.Brown, "The history of power transmission by radio waves," IEEE Transaction on Microwave Theory and Techniques. Vol.MTT-32, 1984, pp 1230-1242
- [42] J.O.Mcspadden, L.Fan, K. Chang. "Design and Experiments of a High-Conversion-Efficiency 5.8 GHz Rectenna", IEEE Transactions on Microwave Theory and Techniques, VOL. 46, NO.12, 1998 pp 2053-2060
- [43] W.C. Brown and E. Eugene Eves, "Beamed Microwave Power Transmission and its application to space", IEEE Transactions on Microwave Theory and Technique, Vol40, NO.5, 1992, pp 1239-1250
- [44] P.E. Glaser, "Power from the sun; Its future," Science, vol. 162, 1968, pp 857-886
- [45] N. Shinohara, H. Matsumoto, "Experimental study of large rectenna array for microwave energy transmission", IEEE Transaction on Microwave Theory and Techniques, VOL.46, NO.3, 1998, pp 261-268
- [46] Y.-J. Ren, M.-Y. Li, and K. Chang, "35 GHz rectifying antenna for wireless power transmission", Electronics Letters, Vol 43, Issue 11, pp 602-603
- [47] J. Zbitou, M. Latrach, "Hybrid Rectenna and monolithic integrated Zero-Bias Microwave Rectifier", IEEE Transactions on Microwave Theory and Techniques, VOL. 54, NO.1, 2006, pp147-152
- [48] J.A.G Akkeermans, M.C. van beurden, G. J.N. Doodeman and H.J. Visser. "Analytical Models for Low-Power Rectenna Design", IEEE Antennas and Wireless Propagation Letters, VOL. 4, 2005, pp 187-205

- [49] C.A. Balanis, Advanced Engineering Electromagnetic, John Wiley & Sons, New York, 1989
- [50] I. J. Bahl and P.Bhartia, Microstrip Antennas, Artech House, Dedham, MA, 1980
- [51] E.O. Hammerstad, "Equations for Microstrip Circuit Design", Proc. Fifth European Micro-wave conf., 1975, pp. 268-272
- [52] K.R. Carver and J.W. Mink, "Microstrip Antenna Technology," IEEE Transactions on Antenna and propagation, Vol. AP-29, No.1, 1981, pp 25-27
- [53] R. E. Collin, Foundations for Microwave Engineering, Chapter 6, McGraw-Hill Book Co., New York, 1992
- [54] A. G.Derneryd, "A Theoretical Investigation of the Rectangular Microstrip Antenna Element," IEEE Transactions on Antennas and Propagation, Vol.Ap-26, NO. 4, 1978, pp 532-535
- [55] W.f. Richards, "Microstrip Antennas," Chapter 7 in Antenna Engineering Handbook (R.C Johnson and H. Jasik, eds), McGraw-Hill Book Co., New York, 1984
- [56] A.J. Zaman, R.Q. Lee and R.N. Simons. "A new design approach for a patch antenna with a notch feed", Microwave and optical technology letters, Vol.23, No.4, 1999, pp 236 – 238
- [57] G. Tzeremes, T. S. Liao, P.K.L. Yu and C.G. Christodoulou, "Computation of equivalent circuit models of optically driven CPW-Fed slot antennas for wireless communications", IEEE Antennas and wireless propagation letters, Vol. 2, 2003, pp 140-142

- [58] M. Hamid and R. Hamid, "Equivalent Circuit of dipole antenna of arbitrary length", IEEE Transactions on antennas and propagation, Vol. 45, No. 11, 1997, pp 1695-1696
- [59] T.G. Tang, Q.M. Tieng, and M.W. Gunn, "Equivalent Circuit of a dipole antenna Using Frequency-Independent Lumped Elements", IEEE Transactions on Antennas and Propagation, Vol. 41, No. 1, 1993, pp 100-103
- [60] GR. DeJean, M.M. Tentzeris, "The application of lumped element equivalent circuits approach to the design of single-port microstrip antennas", IEEE Transactions on Antennas and Propagation, Vol.55, NO.9, 2007, pp2468-2472
- [61] H. Li, G. Subramanyam, "Performance of Thin Film Ferroelectrics as EMC Decoupling Capacitors", Submitted to IEEE transactions on Ultrasonics, Ferroelectrics, and Frequency Control.
- [62] H.M. Chen, J.M. Lan, J.L. Chen, and J.Y.M Lee. "Time-dependent and trap related current conduction mechanism in ferroelectric $\text{Pb}(\text{Zr}_x\text{Ti}_{1-x})\text{O}_3$ films", Applied Physics Letter, 69(12), 1996, pp 1713-1715
- [63] A. Lisauskas, S. I.Khartsev, and A.M. Grishen. "Impedance fluctuation in epitaxial PZT films". Integrated Ferroelectrics, Vol. 38, 2001, pp 3-12
- [64] I.Stolichnov and A.Tagantsev. "Space-charge influenced-injection model for conduction in $\text{Pb}(\text{Zr}_x\text{Ti}_{1-x})\text{O}_3$ thin film", Journal of Applied Physics, Vol.84, Number 6, 1998, pp 3216-3225
- [65] C.Sudhama, A.C. Campbell, P.D. Maniar, R.E. Jones, R.Moazzami, and C.J.Mogab,"A model for electrical conduction in metal-ferroelectric-metal thin film capacitors", Journal of Applied Physics, 75(2), 1994, pp 1014-1022

- [66] V. Buscaglia, M.T. Buscagila, Viviani, M. Mitoseriu, L. Nanni, P. Trefiletti, P. Piaggio, I. Grogora, T. Ostapchuk, J. Pokorny, J. Petzelt, "Grain Size and grain boundary-related effects on the properties of nanocrystalline barium titanate", *Journal of the European Ceramic Society*, 26 (14), pp 2889-2898
- [67] G. Arlt, D. Hennings, G. De, "Dielectric properties of fine-grained barium titanate ceramics", *J.Appl. Phys*, 58, 1985. pp 1619-1625
- [68] G. Ahmad, M B.Dickerson, Y Cai, S.E. Jones, E M.Ernst, J.P.Vernon, M.S. Haluska, Y.Fang, J. Wang, G. Subramanyam, R.R. Naik, and K.H. Sandhage, "Rapid Bioenabled Formation of Ferroelectric BaTiO₃ at Room Temperature from an Aqueous Salt Solution at Near Neutral pH", *Journal of American Chemistry Society*, Vol 130, pp 1-4
- [69] H Jerry, Z Yu, D Ravi, "Epitaxial BaTiO₃ films on silicon for MFSFET applications", *Integrated Ferroelectrics*, Vol 27, 1999, pp 41-50
- [70] S Frank, P Poncharal, ZL Wang, WA de Heer. "Carbon nanotube quantum resistors", *Science*, Vol: 280, Issue:5370, pp 1744-1746
- [71] P.Li, T.-M. Lu. "Conduction mechanisms in BaTiO₃ thin films", *Phys.Rev, B* Vol 43, pp 14261-14264
- [72] S.M.Sze, *Physics of Semiconductor Devices*, Wiley, New York, 1981, pp 402-403.
- [73] RJ Cava, WF Peck, JJ Krajewski, "Compensation of the temperature coefficient of the dielectric constant of barium strontium titanate", *Applied Physics Letters*, Vol: 67, Issue: 25, 1995, pp 3813-3815

[74] XY Zhou, DY Wang, LX He, "Influence of temperature on the in-plane dielectric properties of barium strontium titanate thin films", *Integrated Ferroelectrics*, Vol 77, 2005, pp 157-164

[75] E.N. Bunting, G.R. Shelton, A.S. Creamer, "Properties of Barium-Strontium Titanate Dielectrics", *Journal of the American Ceramic Society*, Vol.30, 1947, pp 114-116

[76] J McAneney, LJ Sinnamon, RM Bowman, JM Gregg, "Temperature and frequency characteristics of the interfacial capacitance in thin-film barium-strontium-titanate capacitors", *Journal of Applied Physics*, Vol 94, 2003, pp 4566-4570

Appendices

Matlab code for designing patch antenna

```
% Design of rectangular patch
%E is the effective permittivity of the substrate
%W is the width of the rectangular patch with the unit of cm
%L is the actual length of the patch
%Delta_L is the extended incremental length of the patch
function [E,W,L,Delta_L]=patch(e,f,h)
%f is the resonant frequency with the unit of GHz
%e is the relative permittivity of the substrate
%h is the height of the substrate with the unit of cm
W=(30/(2*f))*sqrt(2/(e+1))
E=(e+1)/2+((e-1)/2)/(sqrt(1+12*h/W))
Delta_L=h*0.412*(E+0.3)*(W/h+0.264)/((E-0.258)*(W/h+0.8))
L=30/(2*f*sqrt(E))-2*Delta_L
```

Matlab code for designing notch feed patch antenna with characteristic impedance

```
% This programme is to calculate the feed line width of the antenna by
% matching the patch antenna using a microstrip-line feed whose
```

% characteristic impedance

ezplot('(60/sqrt(2.2))*log((8*0.1588)/x+x/(4*0.1588))-50',[0,1])

function y=final(x)

L=0.906;

microstrip;

y=Rin*cos(pi*x/L)-50

function y1=l2(x)

W=1.186;

L=0.906;

h=0.1588;

lamda=30/10;

k0=2*pi/lamda;

y1=((sin(k0*W*cos(x)/2)./cos(x)).^2).*besselj(0,k0*L*sin(x)).*(sin(x)).^3;

function y=l1(x)

W=1.186;

L=0.906;

h=0.1588;

lamda=30/10;

k0=2*pi/lamda;

y=((sin(k0*W*cos(x)/2)./cos(x)).^2).*sin(x).^3;

function y=impedance1(x,h,relative_epsilon)

y=(60/sqrt(relative_epsilon))*log((8*h)/x + x/(4*h))-50

```

function y=impedance2(x,h,relative_epsilon)

y=(120*pi/(sqrt(relative_epsilon)*(x/h+1.393+0.667*log(x/h+1.444))))-50

lamda=30/10;

k0=2*pi/lamda;

W=1.186;

L=0.906;

h=0.1588;

relative_epsilon=2.2;

Q1=quad(@l1,0,pi);

G1=Q1/(120*pi^2)

Q2=quad(@l2,0,pi);

G2=Q2/(120*pi^2)

Rin=(1/(2*(G1+G2)))

f=@(x) (Rin*((cos(pi*x/L))^2)-50);

y=fzero(f,0.3)

ezplot('228.3508*((cos(pi*x./0.906)).^2)-50',[0,1])

function y=l1(x)

y=((sin(k0*W*cos(x))/cos(x))^2)*(sin(x))^3

```

VITA

Aug. 23, 1984	Born in Xi'an, Shaanxi, China
2006	BEng, Electrical Engineering, Xi'an Jiaotong University, China
2008	M.S., Electrical Engineering, University of Dayton

PUBLICATIONS

- [1] J. Wang, G. Subramanyam, and H. Li, "Comparison of AC and DC resistance of PZT and its related electrical model", to be presented in the International Symposium on Integrated Ferroelectrics 2008, Singapore, Jun. 2008.
- [2] H. Li, J. Wang, and G. Subramanyam, "Impedance of Ferroelectric Varactor Shunt Switches", to be presented in the International Symposium on Integrated Ferroelectrics 2008.
- [3] H. Li, G. Subramanyam, and J. Wang, "Performance of thin film ferroelectrics with dopant ion charges", to be published in the special issue of Integrated Ferroelectrics, ISIF 2007, Dec. 2007.

R002593838

[4] H. Li, G. Subramanyam, and J. Wang, "Capacitance of Thin Ferroelectric Thin Films Obtained by Different Methods", presented in the IEEE International Symposium on Applications of Ferroelectrics, ISAF 2008, Feb. 2008.

[5] G. Ahmed, M. Dickerson, Y. Cai, S. Jones, E. Ernst, M. Haluska, J. Wang, G. Subramanyam, R. Naik, N. Kroger, and K. Sandhage, "Rapid bio-enabled formation of ferroelectric BaTiO₃ at room temperature from an aqueous salt solution at near neutral pH", Journal of American Chemical Society, Vol. 130, NO. 1, pp 4-5.